ELSEVIER DEVELOPMENTS IN VOLCANOLOGY 8

VESUVIUS

EDUCATION, SECURITY AND PROSPERITY

EDITED BY
FLAVIO DOBRAN

Elsevier
Radarweg 29, PO Box 211, 1000 AE Amsterdam, The Netherlands
The Boulevard, Langford Lane, Kidlington, Oxford OX5 1GB, UK

First edition 2006

Library of Congress Cataloging-in-Publication Data
A catalog record for this book is available from the Library of Congress

British Library Cataloguing in Publication Data
A catalogue record for this book is available from the British Library

ISBN-13: 978-0-444-52104-0
ISBN-10: 0-444-52104-6

Printed and bound in The Netherlands

06 07 08 09 10 10 9 8 7 6 5 4 3 2 1

CONTENTS

Chapter 2

Education: Cognitive Tools and Teaching Vesuvius
F. Dobran

Chapter 3

Social and Economic Reality of Vesuvius Area

V. Di Donna

Chapter 4

Geophysical Precursors at Vesuvius from Historical and Archeological Sources
A. Marturano

Chapter 5

Ballistics Shower During Plinian Scenario at Vesuvius
V. De Novellis and G. Luongo

Chapter 6

Shear-Wave Velocity Models and Seismic Sources in Campanian Volcanic Areas: Vesuvius and Phlegraean Fields
M. Guidarelli, A. Zille, A. Saraò, M. Natale, C. Nunziata and G.F. Panza

Chapter 7

Global Volcanic Simulation: Physical Modeling, Numerics, and Computer Implementation

F. Dobran and J.I. Ramos

PREFACE

Vesuvius is today surrounded by a densely populated area. Within a radius of 10 km of the crater live about one million people and within this distance and 50 km live another two million people, with the city of Naples being situated between Vesuvius on the east and the Phlegraean Fields on the west. In the last 20 000 years, this volcano has produced many plinian and smaller scale eruptions, and is most famous for its eruption in 79 A.D. when it buried the Greco-Roman towns of Pompeii and Herculaneum. Its 1631 subplinian eruption was even more devastating for the surrounding territory and for the first time made an important imprint on the Europeans during the Age of Reason or Enlightenment in the seventeenth and eighteenth centuries. Following this eruption, Vesuvius remained active until 1944 with its many strombolian and lava flow eruptions. Since 1944, the presence of smoke has disappeared and the surrounding territory began to be veiled in asphalt and concrete, with the smoke remaining a postcard memory and the eruptions a distant foreboding.

Vesuvius sleeps today and only some faint fumaroles within the crater and low-level seismic activity below its cone suggest that this mountain of fire is preparing for another of its colossal eruptions that could affect hundreds of thousands, if not millions, of people. Computer simulations predict that there is a high probability of a subplinian or plinian eruption occurring in the twenty-first century. For five centuries or more before the eruptions of 79 A.D. and 1631, the volcano remained quiescent and the people became complacent as the memory of past eruptions was gradually forgotten. A similar situation can occur again. Indeed, according to *Osservatorio Vesuviano* in Naples and its parent institution *Istituto Nazionale di Geofisica e Vulcanologia* in Rome '*Tutto è sotto controllo*' ('everything is under control'), thanks, so they claim, to the instruments that monitor the volcano and an evacuation plan that will allow everybody to escape on time during an emergency. This is, of course, an illusion due to the difficulty of separating tectonic from volcanic events, rapid rise of magma when the premonitory signals become clear that the volcano is erupting, and gross unreliability of the evacuation plan which to date has produced little peace of mind to many Vesuvians and no social and cultural progress that would emancipate hundreds of thousands of people from their difficult predicament. Meanwhile, the population around the volcano is becoming more complacent and many are convinced that Vesuvius will not erupt again. While it would be erroneous to promote a policy of eminent danger when this danger does not exist, it is equally erroneous to promote a policy of inaction, especially since we know that it is only a matter of time before Vesuvius wakes up.

A decade ago an interdisciplinary project called VESUVIUS 2000 was proposed for the Vesuvius area. Unlike evacuation plans which tend to manage emergencies, this initiative aims at preparing the territory around Vesuvius to confront volcanic emergencies with minimum socio-economic and cultural consequences. What Vesuvians need is not so much a plan that tells them where to run in the event of an

eruption, but the creation of an environment that offers security from future eruptions. VESUVIUS 2000 aims at achieving this objective while, at the same time, reducing the current state of social decay that is associated with limited economic opportunities. The danger from the volcano can be taken to advantage for producing a whole new secure and prosperous habitat for the people surrounding Vesuvius. The current evacuation plan has produced an unprecedented damage to the Vesuvius area, and, as long as it is being used as an instrument that only benefits special groups, there will be no prosperity for Vesuvians and these people will have to depend on their St. San Gennaro for protection. Since 1995, many Vesuvians have been educated on different risk management plans for the territory, but neither Italy nor the European Union has taken the Vesuvius problem seriously. Since Vesuvius is 'under control' why bother to produce a safer and more prosperous habitat for Vesuvians?

A forum on VESUVIUS 2000, held on 2 and 3 September 2004 in Villa Campolieto in Ercolano, near the ruins of Herculaneum, provided an impetus to complete this book. The forum was attended by over one hundred local and foreign scientists, educators, students, and some authorities and lay people from the Vesuvius area. Its principal organizers, besides myself and members of my organization GVES, were Giuseppe Luongo, Giuliano Panza, and Bernadette de Vanssay from the Universities of Naples, Trieste, and Paris V, respectively. The first day of the forum involved technical sessions and the second one excursions to the ruins of Pompeii and Villa Augustus on the opposite side of the Monte Somma relief. The presentations at the forum were multidisciplinary and dealt with the structure of the volcanic system, modeling of eruption processes, education, socio-economic conditions, and civil protection. The excursions to Pompeii and Villa Augustus clearly demonstrated our fragility and weakness when confronting nature and our complacency with danger.

This book should be useful to professionals and nonprofessionals alike, and, especially, to the populations of the Vesuvius area and other places around the world that face similar problems. It should also prove useful to those who want to familiarize themselves with the geographical, social, and cultural settings of the area, as well as to those who wish to know about the current understanding of the substructure of the volcanic system, the objectives of global volcanic simulation, and difficulties involved in managing risk in densely populated areas. The book should also be useful to educators, who teach primary, intermediate, and secondary school children and students about their environment, and volcanoes in particular.

Because of the multidisciplinary issues considered here, students, professionals, lay public, and civil protection managers should find in this volume sufficient information for further study, elaboration of topics, or adaption to their particular situations. The objectives of VESUVIUS 2000 need to be diffused to an audience beyond the Vesuvius area, for critical evaluation and comparison with analogous initiatives. We cannot embark on a serious path of risk mitigation in a densely populated area unless we fully understand the history, culture, and socio-economic conditions of the area and are willing to scrutinize every detail of our intended actions and fully expose our projects to constructive criticism. A mitigation and risk

management plan which is hidden from the public, and its architects refuse to discuss it publicly and away from professional audience, does not serve any useful purpose, especially for those living in the close proximity of Vesuvius.

The book is divided into seven chapters, with each chapter providing a summary in both English and Italian. Following this preface, the book provides an extended summary of VESUVIUS 2000 in Italian. The Appendix of Chapter 2 is in Italian and provides a global perspective of the territory as seen by a group of intermediate students of the Vesuvius area. The Appendix of Chapter 3 is the Italian version of this chapter. The color versions of black and white figures of in Chapter 2 are collected at the end of the book, and the extensive Notes in Chapters 1 and 2 elaborate on the historical, cultural, and scientific aspects of the area and beyond.

Chapter 1 presents the difficulties associated with the management of volcanic risk in the Vesuvius area and the principal objectives of VESUVIUS 2000 which aim at transforming the area into a secure and prosperous region. The topics in this chapter deal with Vesuvius consciousness, security culture barriers, habits of mind that prevent the Vesuvians from judging different risk reduction strategies, the grand challenge associated with the protection of people and territory from the volcano, and VESUVIUS 2000 objectives and methodologies. VESUVIUS 2000 is divided into three interrelated topics: Physical environment, which deals with the development of Global Volcanic Simulator and its use for assessing the effects of different eruption scenarios; population, which addresses the social, economic, and educational issues of the people; and territory, which deals with the area infrastructures, urban planning, and civil protection.

Education of children and adults so that they become Vesuvius-conscious citizens is discussed in Chapter 2. Different age groups of students imagine things differently, and it is the aim of education to take advantage of those tools which produce the greatest developments in children. This chapter thus addresses the cognitive tools available to us and how these tools can be used to educate the primary, intermediate, and secondary school children about Vesuvius. We, therefore, discuss educational ideas, kinds of understanding, educational methods, and teaching methodologies. Educating adults about Vesuvius is also important, especially in decreasing their technological illiteracy, because this is preventing many from seeing how the modern technology can liberate them from their difficult predicament. As examples, we discuss several educational efforts in the Vesuvius area, including those from schools, nonprofit and professional organizations, lay public, and others.

The social and economic reality of the Vesuvius area is addressed in Chapter 3. Eighteen communities of more than 500 000 people border the crater of the volcano and, during the last decade, some 30 000 people have left the area for better opportunities and lower risk elsewhere. The educational level of most people living near the volcano is low and, officially, only one-fifth of the population works. Their main economic activities are services, scattered agriculture, and some manufacturing. This kind of environment breeds crime and offers few bright prospects for future generations.

Chapter 4 presents geophysical precursors of Vesuvius from historical and archeological sources. The eruption of Vesuvius in 79 A.D. was preceded by a large magnitude earthquake in 62 A.D. that caused an extensive damage. This and several other events thereafter suggest that the towns surrounding the volcano experienced significant problems before this famous eruption. The eruption of 1631 was also preceded by seismic activity for several hours, and perhaps for a longer time. The last significant earthquake occurred in 1999 and the recent seismicity has been maintained below the magnitude 4 on the Richter scale.

The characteristics of ballistic debris emitted from Vesuvius during the eruption of 79 A.D. are discussed in Chapter 5. This debris, with block sizes of up to 1 m, is common in the deposits of this eruption and reached distances in excess of 10 km from the crater. Modeling of the ballistic shower is, however, in its infancy and not reliable enough to be used today as a tool for the hazard assessment associated with this kind of material being ejected from the volcano.

Our current understanding of the substructure of Vesuvius and that of the nearby Phlegraean Fields is presented in Chapter 6. This understanding comes from the natural seismicity of the volcano and seismic tomography experiments that have been conducted in the 1990s. At that time, I was one of the promoters of such experiments for collecting data that could be used for the validation of Global Volcanic Simulator. Since then, many such studies have been made and their results suggest that both the Vesuvian and Phlegraean areas have low seismic wave velocity layers at a depth of about 10 km and that, therefore, there is no evidence of magma in the superficial regions of the volcano. According to these works, the volcanic conduit is currently sealed and magma resides in a diffused crustal magma reservoir which is fed by a regional one within the uppermost mantle.

Global Volcanic Simulator is the key tool for both ascertaining the effects of different eruption scenarios on the territory surrounding the volcano and producing a new habitat for Vesuvians where they can live safely from future eruptions. In Chapter 7, we discuss physical modeling, numerical, and computer implementation issues related to the development of such a simulator. We have already developed several useful models for simulating magma chamber dynamics and magma ascent in volcanic conduits, and are currently developing a nonequilibrium multiphase and multicomponent atmospheric dispersion model and its associated computer code. This model accounts for two-way turbulence coupling between the gaseous and particulate phases, condensation and evaporation of volatiles, aggregation and fragmentation of pyroclasts, and chemical reactions among the components of different phases. Our objective is to resolve the effects of pyroclastic flows on small and large structures located on the territory surrounding the volcano, determine the fallout characteristics of tephra and ballistic blocks, and ascertain the consequences of plinian plumes transporting the volcanic debris high into the stratosphere during and after an eruption. A practical global simulator must be able to simulate different eruption scenarios and determine their effects on the people and infrastructures, with and without engineering measures aimed at protecting the area surrounding the volcano.

During the last decade, we have only made a modest progress in achieving the objectives of VESUVIUS 2000, because of a politicized evacuation plan that distances independent initiatives and stifles collaboration on this volcano. We have made, however, a significant effort in promoting education and collaboration, and managed to involve many schoolteachers and their students on different topics associated with Vesuvius. Regretfully, the people's representatives in Italy are using the flawed evacuation plan as an instrument for discharging their own responsibility, while the institutions of higher learning and research centers are not sufficiently responsive to help design a safe and prosperous habitat for Vesuvians. We need to get rid of negative habits of mind and force ourselves beyond our personal interests and traditions, and thus attempt to construct a higher level of civilization. VESUVIUS 2000 proposes a technologically-grounded approach to territorial risk management which is dramatically different from other plans. As a consequence, it needs time to bear fruit to the people whose ancestors are the founders of Western Civilization.

Flavio Dobran
January 2006

ACKNOWLEDGMENTS

Many individuals helped to make this book possible. I especially value the support from ordinary people and schoolteachers of the Vesuvius area, because many of them have shown more pragmatism than many of the so-called experts when it comes to managing volcanic risk. For many years, I have enjoyed working on the territory with Giuseppe Luongo. He has been an important supporter of interdisciplinary collaboration and has helped with many seminars. Giuliano F. Panza has also provided a crucial help in this endeavor and measures up to the highest standards of Italian academicians.

The development of a volcanic simulator requires vision, extraordinary experience, and dedication, and I am fortunate to have Juan I. Ramos working with me on this project. My associates of the Vesuvius area, Ida Mascolo, Gelsomina Sorrentino, Tullio Pucci, Annamaria Imperatrice, Arturo Montrone, Anna Ibello, Antonio Longobardi, and Gennaro di Donna, best understand its environment and its people. Without them, it would have been difficult to work on the territory. This book is dedicated to them and others like them who are making a truly civil progress in the Vesuvius area.

I am grateful to Giuliano F. Panza, Lionel Wilson, Mariano Garcia Fernandez, Juan I. Ramos, Giuseppe Luongo, Elena Cubelis, Luis F. Romero Gómez, and Mariangela Guidarelli for reviewing some of the technical material of the book. The objectives of VESUVIUS 2000 in Chapter 1 were scrutinized by lay public, schoolteachers and students, and professionals through more than 150 seminars given in the Vesuvius area since 1994. My associates reviewed some parts of Chapter 2 on education. Antonio Vallario is acknowledged for supporting the work presented in Chapter 3. The Laboratory of Seismology of *Osservatorio Vesuviano* and particularly E. Del Pezzo and P. Ricciolino are acknowledged for providing the waveforms of Vesuvian and Phlegraean Fields seismicities for the analysis presented in Chapter 6. Luis F. Romero Gómes is thanked for his contribution on computer implementation in Chapter 7.

During the preparation of the book I benefited from the help received from Ida Mascolo, Gennaro di Donna and Annamaria Imperatrice. For permissions to publish school works, I am grateful to *Istituto Tecnico Commerciale Luigi Sturzo* of Castellammare di Stabia, *Squola Media Statale Rocco Scotellaro* of Ercolano, *Scuola Media Statale Orazio Comes* of Portici, *Istituto Comprensivo Statale Franscesco d'Assisi* of Torre del Greco, and *Scuola Materna IV Circolo* of Portici. Additional material on education was provided by Tullio Pucci, Arturo Montrone, Francesco Langella, Gennaro Di Donna, Annamaria Scorza, Annamaria Imperatrice, Gianfranco Gambardella, Elvira Maddaluno, Giuseppe Sbarra, Annamaria Trotta, and Leonardo Limocia. For permissions to publish their works, special thanks are due to Gianfranco Gambardella for his clock art preceding Chapter 2, Paolo Schettino for his two poems in Chapter 2, *Istituto Geografico Militare Italiano* for the aerial photograph of the Vesuvius area, and ARC Science Simulations,

Smithsonian Institution, and UNAVCO for the two images of the world and Italy preceding Chapter 1. Lastly, I am also grateful to Friso Veenstra of Elsevier and to the production Team of Macmillan India Limited for bringing this book to the attention of readers worldwide.

Flavio Dobran

Vesuvius
F. Dobran (Editor)

Chapter 7

Global Volcanic Simulation: Physical Modeling, Numerics, and Computer Implementation

F. Dobran and J.I. Ramos

Considerate la vostra semenza: fatti non foste a viver come bruti, ma per seguir virtute e conoscenza.

— Dante, iXXVI

ABSTRACT

Physics-based, efficient and reliable simulations of the effects of volcanic eruptions on the surrounding territories are not feasible today. This is, in part, due to the difficulty of incorporating all relevant volcanic and atmospheric processes that occur in a volcanic eruption into an all-inclusive multiphase and multicomponent physical model. But, even if such a model were available, there would also be difficulties in solving the resulting mathematical equations accurately and efficiently, and with enough spatial and temporal resolution, on current computers. Global volcanic simulation requires incorporating different types of models into a simulation package or Global Volcanic Simulator. These models include those pertaining to magma chamber dynamics, opening of volcanic conduits, magma ascent, and atmospheric dispersion of pyroclasts. During the past decade, we have developed several such models which are described elsewhere. As these models have disparate time and length scales, each must be carefully verified and validated before it can be integrated into the global simulator. This chapter presents our work on a new pyroclastic dispersion model and its numerical and computer implementation on available computers.

The structural model of multiphase mixtures presented here includes mass, momentum, energy, and turbulence coupling between the gaseous and particulate phases, and its microphysics accounts for the effects of condensation and evaporation of volatiles, fragmentation and aggregation of particulates, formation of precipitation from heterogeneous condensation, and gas–particle–turbulence modulation. The resulting non-equilibrium multiphase and multicomponent flow model includes separate transport equations for each Eulerian and Lagrangian phase of the mixture and an additional set of transport equations that account for the mixture's structural characteristics. This allows for both the coupling between different scales and the exchange of energy between large and small eddies in the plume.

Before implementing a numerical solution methodology, we have carried out detailed studies on the simulation requirements, accuracy of different numerical solvers, and tradeoffs of different parallel computer paradigms. The adopted strategy involves domain decomposition at both the physical and algebraic levels, and second- and third-order accurate numerical discretization schemes for the advection terms, multiblock grids, and iterative Krylov subspaces methods that are suitable for implementation on multiprocessor environments. This strategy permits simulations of high rising and widely dispersing plinian columns as well as of those columns that collapse and produce pyroclastic flows and surges. Following the current verification stage, the resulting physico–mathematical–computer model will be validated with data from several well-known eruptions, including those from Vesuvius, before other models for the magma chamber dynamics, opening of volcanic conduits, and magma ascent are incorporated into a global simulation package for the prediction of volcanic eruptions. The resulting Global Volcanic Simulator will be employed for achieving some of the key objectives of the VESUVIUS 2000 project.

RIASSUNTO

Simulazioni, basate sui principi della fisica, efficienti ed attendibili, degli effetti delle eruzioni vulcaniche sul territorio circostante non sono attualmente possibili. Questo è in parte dovuto alla difficoltà di includere tutti i processi vulcanici ed atmosferici rilevanti, che si verificano durante una eruzione, in un unico modello fisico multifase e a molte componenti. Ma, anche se tali modelli fossero disponibili, ci sarebbero delle difficoltà nel risolvere, con i computer ora disponibili, in modo accurato ed efficiente e con sufficiente risoluzione spazio-temporale, le equazioni matematiche risultanti. La simulazione globale del vulcano richiede l'inserimento di diversi modelli in un pacchetto di simulazione ovvero in un Simulatore Vulcanico Globale. Questi modelli comprendono quelli relativi alla dinamica delle camere magmatiche, alla apertura dei condotti vulcanici, alla risalita del magma ed alla dispersione nell'atmosfera dei prodotti piroclastici. Negli ultimi dieci anni, sono stati sviluppati alcuni di questi modelli che sono descritti in altre pubblicazioni. Poiché questi modelli hanno scale spazio-temporali alquanto disparate, ciascuno di essi deve essere attentamente verificato e convalidato prima di poter essere incluso nel Simulatore Globale. Questo capitolo descrive lo sviluppo di un nuovo modello di dispersione piroclastica e la sua implementazione numerica sui calcolatori disponibili attualmente.

Il modello strutturale delle miscele multifase presentato in questa sede comprende l'accoppiamento di massa, momento, energia e turbolenza tra le fasi gassosa e particolata, e la relativa microfisica tiene conto degli effetti di condensazione ed evaporazione dei volatili, frammentazione ed aggregazione del particolato, formazione della precipitazione dovuta a condensazione eterogenea, e modulazione della turbolenza gas–particella. Il risultante modello di flusso multifase e multicomponente comprende equazioni di trasporto separate per ciascuna fase Euleriana e

Lagrangiana della miscela ed un ulteriore insieme di equazioni di trasporto, che tengono in conto le caratteristiche strutturali della miscela stessa. Ciò permette sia l'accoppiamento fra diverse scale sia lo scambio di energia fra vortici piccoli e grandi nel pennacchio.

Come passo preliminare alla implementazione di una metodologia basata su soluzioni numeriche, è stata realizzata una serie di studi dettagliati sui requisiti della simulazione, accuratezza dei diversi risolutori e compromessi tra i paradigmi di diversi calcolatori paralleli. La strategia adottata richiede la decomposizione del dominio sia a livello fisico che algebrico, e la costruzione di schemi accurati di discretizzazione al secondo ed al terzo ordine per i termini di advezione, griglie multiblocco, e metodi iterativi nei sottospazi di Krylov, che sono adatti per la realizzazione dei codici in ambiente a multiprocessore. Questa strategia permette la simulazione sia di colonne pliniane molto elevate e molto disperse che di quelle che collassano e producono flussi piroclastici e surges. Completato lo stadio di verifica, il modello fisico–matematico–numerico risultante sarà validato utilizzando dati di svariate eruzioni ben conosciute, comprese quelle del Vesuvio, prima che altri modelli per la dinamica delle camere magmatiche, l'apertura dei condotti vulcanici e la risalita del magma siano incorporate nel pacchetto per la simulazione globale per la previsione di eruzioni vulcaniche. Il Simulatore Vulcanico Globale sarà utilizzato per realizzare alcuni degli obiettivi chiave del progetto VESUVIUS 2000.

7.1. INTRODUCTION

Hundreds of thousands of people in Mexico, the Philippines, Japan, Indonesia, Italy, and other underdeveloped and developed countries live very close to some of the most dangerous volcanoes. For example, within a radius of 10 km of the Taal volcano in the Philippines live about 200 000 people and within 20 km, 500 000 people. Within 10 km of the Galeras volcano in Colombia live some 300 000 people, and within 20 km of Fuji in Japan and Popocatepetl in Mexico live 500 000 and 200 000 people, respectively. Within a radius of 10 km of Vesuvius live about 1 million people and within 20 km more than 2 million people. In the nearby Phlegraean Fields, the situation is similar, and a large-scale eruption at either of these places would affect, at least, 3 million people who reside on the Campanian plain. The main hazards from these Neapolitan volcanoes are the fall of ash and large blocks, pyroclastic flows, mudflows, and avalanches. Sakurajima in Japan, Mayon in the Philippines, Santa Maria in Guatemala, and Mt. Rainier in the United States pose analogous risks to densely populated areas, including the potential for producing catastrophes, massive human displacements, and losses of property in the event of large-scale eruptions.

People can live safely and in harmony with volcanoes only if their potential danger can be reliably assessed and measures taken to convince the public that it is safe to live at sufficient distances from the craters. Ash fall from an eruption can affect thousands of square kilometers, while the pyroclastic flows and mudflows can destroy everything on their paths in a matter of minutes unless adequate protection

measures have been placed into effect. If inadequately protected, people's dwellings and city infrastructures can be wiped out and those who manage to escape are forced to start life all over.

What to do with about 1 million Vesuvians and an equal number of those living in the Phlegraean Fields is a problem of unprecedented proportions, and neither the people who are exposed to the danger nor their representatives at local and national governments are taking this problem very seriously. The volcanologists' solution to this problem (Protezione Civile, 1995) is too simplistic and grossly inadequate for this territory, for it envisages the possibility of evacuating hundreds of thousands of people on a short notice and in a probable state of panic albeit in the absence of reliable evacuation infrastructures. Such a policy tends to manage the catastrophe, protects the benefactors of evacuation plan architects, and promotes inaction on the part of people's representatives. VESUVIUS 2000 (Dobran, 2006) works instead in the direction of prevention. Its aim is to use modern technology to produce a new habitat for Vesuvians where they can live in safety and prosperity, and confront future eruptions with minimum socio-economic and cultural consequences. Such a habitat should be sufficiently far from the volcano and adequately protected to sustain the full fury of the volcano.

The key tool for determining the effects of future eruptions on the territory surrounding a volcano is Global Volcanic Simulator (Dobran, 1993, 1994a,b), or a physico–mathematical–computer model of the entire volcanic complex. Such a simulator incorporates physical and chemical models of all conceivable eruption processes within the volcano and in the atmosphere above it, and through a probabilistic analysis determines the likelihood of different eruption scenarios and their consequences on the territory surrounding the volcano (Dobran, 2006). Therefore, the predictions of a Global Volcanic Simulator could be used for urban planning the territories in densely populated areas around volcanoes, developing adequate infrastructure for protecting humans and animals in the event of volcanic eruptions, etc. Such a global volcanic model employs geological and geophysical data pertaining to the origin and composition of volcanic deposits, underground reservoirs of water, magma and lava flows, strength, elasticity and plasticity of magmas, lavas, and surrounding rocks and soils. In the atmosphere, the simulator accounts for mixing and chemical reactions of the material discharged from the volcano with the air constituents, and determines the dispersion of this material in the proximal and distal regions from the vent.

A useful Global Volcanic Simulator of Vesuvius should be able to resolve the effects of tephra fall and pyroclastic flows on different types of structures (such as houses and infrastructures) and track the dispersion of pyroclasts high into the stratosphere and for hundreds of kilometers in lateral directions under different atmospheric conditions for 50 h or more of intermittent and intense volcanic activity. These requirements are extremely demanding from both the physical and the computational perspectives and no current generation pyroclastic dispersion model is able to meet these requirements.

Previous models of pyroclastic dispersions are two-dimensional and contain rather simple physics. For example, the models of Valentine and Wohletz (1989) and Dobran et al. (1993) are two-dimensional velocity and temperature

non-equilibrium two-phase and multiphase flow models, respectively. The latter model is based on a granular kinetic theory which includes a transport equation for the granular temperature and different pressures for the gaseous and solid phases. Both of these models include eddy diffusivity turbulence models for the gas phase, ignore two-way turbulence coupling between the solid and gaseous phases, and lack the necessary microphysics to account for condensation, evaporation, and chemical reactions of plume constituents. The model of Neri and Macedonio (1996) uses the same physics and computer code as the one of Dobran et al. (1993), except that the authors specify two instead of one particle classes in their simulations and do a poor job of verifying the numerical calculations. This granular flow model utilizes a staggered grid and a semi-implicit numerical procedure, and produces unacceptably large numerical diffusion errors for the grids used in the simulations. The model of Dartevelle (2004) is also a granular flow model that is based on the work of Syamlal (1998). It uses the same transport equations to those of Dobran and co-workers and a more complete set of constitutive equations which account for the description of particulate behavior at high particle concentrations. The results pertaining to numerical simulations based on this model and reported in Dartevelle et al. (2004) should, however, be viewed with caution, since the model does not account for condensation which normally occurs soon after the eruption. Oberhuber et al. (1998) and Herzog et al. (1998) adapted a velocity and temperature equilibrium model from meteorology to volcanic plumes. This model accounts for silicate particles through their settling velocities and includes the phase change of water vapor and the growth of cloud droplets, ice crystals, raindrops, and hail-size groupel particles. The interaction between water and silicate particles is ignored and the presence of volcanic gases in the plume is not taken into account. The model includes a transport equation for turbulent kinetic energy of the gas phase, but its limitations arise from the assumptions of mechanical and thermal equilibrium between the phases, the absence of interactions between ash particles and plume hydrometeors, and the neglect of the effects of volcanic gases (such as SO_2, H_2S, and HCl) on plume dynamics and thermodynamics. The model of Ongaro et al. (2004) attempts to extend the model of Dobran et al. (1993) to three-dimensional multiphase flows.

In the early 1990s, the Italian geological and geophysical communities did not continue supporting the development of an effective simulator for Vesuvius, in spite of an intense and productive initial effort (Dobran and Mulargia, 1991; Dobran et al., 1991, 1993, 1994; Dobran, 1992, 1993, 1994a,b, 1995; Dobran and Papale, 1993; Papale and Dobran, 1993, 1994; Giordano and Dobran, 1994; Macedonio et al., 1994; Coniglio and Dobran, 1995; Dobran and Luongo, 1995; Ramos, 1995, 1999; Dobran and Coniglio, 1996) which demonstrated the feasibility of this project. The development of this simulator continued elsewhere and some of its models are described in Dobran (2001) and in this work. The development of such a simulator includes models for the magma chamber dynamics, opening of the volcanic conduit, magma ascent in volcanic conduits, and pyroclastic dispersion.

The magma chamber dynamics model simulates the evolution of magma reservoirs for hundreds or thousands of years and forecasts a subplinian or plinian eruption of Vesuvius in the twenty-first century with a high probability. The opening

of volcanic conduit model accounts for the conditions of magma in magma reservoir and yield stress characteristics of overlying rocks, and predicts a very rapid magma ascent once the instability sets in. Several magma ascent models simulate steady-state, and transient melting and solidification processes in volcanic conduits. These include the effects of gas exsolution, magma fragmentation, and erosion on conduit flow dynamics.

Further use of the pyroclastic dispersion model of Dobran et al. (1993) was abandoned because of its outdated semi-implicit and staggered grid numerical algorithms, which result in unacceptably long computation times and accumulation of numerical diffusion errors. In addition, this model lacks the necessary microphysics associated with phase changes, chemical reactions, and two-way turbulence coupling between the gaseous and solid phases. Our former collaborators are, nevertheless, still using this code as well as other models that were developed in collaboration (Neri and Macedonio, 1996; Ongaro et al., 2002; Todesco et al., 2002; Zuccaro and Ianniello, 2004).

This chapter deals with some of the issues associated with the development of an effective pyroclastic dispersion model for the Global Volcanic Simulator. In Section 7.2, we summarize a multiphase and multicomponent physical model which is considerably different from existing ones. This thermohydrodynamic (velocity, pressure, and temperature) non-equilibrium model includes the effects of phase changes, chemical reactions, aggregation and fragmentation of liquid and solid particles, turbulence coupling between the gaseous phase and particulate matter, and the structural characteristics associated with phase inertia and dilatation and contraction effects. The solution of the resulting modeling equations employs state-of-the-art numerical procedures and domain decomposition (DD) methods for efficient and accurate simulations. The numerical solution procedures and choices for an effective solution of the resulting physico–mathematical model are discussed in Section 7.3. In Section 7.4, we address computer implementation issues for the purpose of producing accurate and effective simulations of plinian and collapsing volcanic columns.

Interactions between volcanic products and atmospheric constituents include different time and length scales which produce both physical and numerical modeling difficulties. Our physical model accounts for the coupling between these scales and our numerical solution strategy is presently being verified to insure that it correctly and efficiently solves the mathematical equations under a wide variety of conditions within an acceptable error tolerance. The subsequent task of validation requires that the mathematical solutions agree with observed physical and chemical processes of eruptions. Only after these two tasks have been carried out satisfactorily can the resulting pyroclastic dispersion model be integrated with the magma chamber and magma ascent models into a simulation package or Global Volcanic Simulator. Poor verification of computer code calculations can only produce damage to the community that lacks the knowledge to evaluate complex multiphase models and the accuracy of the corresponding numerical calculations. Too many technical papers and reports approach the issues of verification and validation in a haphazard and piecemeal manner (Roache, 1998a).

7.2. PHYSICAL MODELING

7.2.1. Products of volcanic eruptions

Volcanic eruptions produce different size particles and many volatile and gaseous species which are originally dissolved in the magma and bonded in different minerals. One can observe eruptions directly and sample the plume or measure the products on the ground during or after the eruption. The results from these two approaches can be different, however, because of the aggregation processes which tend to produce clusters of fine particulates and fragmentation processes that produce fine particulates from large particles. These clusters usually fall closer to the vent than the particulate matter from which the clusters are made or their dispersion depends of their size and processes within the plume. Explosive volcanic eruptions have extremely varied characteristics (Walker, 1981; Cas and Wright, 1993).

The pyroclastic deposits contain juvenile fragments from the breakup or fragmentation of magma, glasses and crystals from rapid cooling of magma in conduits and atmosphere, and lithic fragments from the erosion of rocks pertaining to the volcanic edifice itself. These products have different densities and shapes and thus contribute to particulate fractionation. Lithic fragments tend to be coarser than the associated juvenile products and, therefore, tend to fall out from the eruption column close to the vent. Due to the moisture, electrostatic forces in the atmosphere, and the large surface area/mass ratio of glass fragments, the fine ash (less than about 50 mμ) can aggregate into particles of several hundred microns and thus also fall close to the vent and hence contribute to the multimodal spectrum of ash particles that is observed in many field deposits (Carey and Sigurdsson, 1982; Brazier et al., 1983; Rose et al., 1983).

A wide variety of volcanic processes can produce these products. Inside volcanos, magmas with different chemical compositions fractionate and cool in the magma reservoirs or chambers before ascending toward the surface through different types of fissures, fractures and conduits that may or may not be surrounded by underground aquifers. Magma can interact with water in these aquifers and thus produce phreatomagmatic eruptions that release large quantities of water which can act as a binding agent for particle aggregation (Veitch and Woods, 2001; Textor and Ernst, 2004).

Poorly degassed silicic magmas (such as dacites and rhyolities) fragment in conduits and exsolve volatile species (including trace metals) as they ascend toward the surface. Many of these fragments subsequently break up into smaller ones through collisions and interactions among themselves and with conduit walls. Some volatile species condense as they ascend and are adsorbed on the particulates. Once discharged into the atmosphere, the fragmented and exsolved magmatic species interact among themselves and with the gaseous, solid, and liquid phases, and thus contribute to the dissolution of species into the aqueous phase, gas–particle reactions, aqueous phase reactions, fragmentation and agglomeration of solid and liquid particles, and so on. Reviews of some of these processes are available in Robock (2000), Dobran (2001), and Mather et al. (2003).

Volcanic processes also release large quantities of gases which are dominated by water vapor (H_2O), carbon dioxide (CO_2), and sulfur dioxide (SO_2). These are followed by smaller concentrations of hydrogen (H_2), hydrogen sulfide (H_2S), hydrochloric acid vapor (HCl), hydrogen fluoride (HF), carbon monoxide (CO), and many other elements and compounds which contribute to the aerosol budget of the volcanic plume (Symonds et al., 2001; Mather et al., 2003).

Once discharged into the atmosphere, the emissions are cooled, diluted, and oxidized by air. There, they trigger a complex set of reactions (Ammann and Burtscher, 1993) and produce aerosols of liquid and solid particles. The aerosols aggregate into cloud condensation nuclei on which rain droplets are formed (Wagner, 2000). Volcanic H_2O vapor, CO_2, and HF are stable, H_2 and CO oxidize to H_2O and CO_2, respectively, and the sulfur compounds react with water to produce sulfuric acid (H_2SO_4) aerosols (Laaksonen, 2000). These aerosols can then react with nitrogen oxides (NOx) to produce nitric acid (HNO_3) gas which lowers the critical supersaturation for droplets and thus increases the number of activated droplets (AGU, 1992; Brasseur and Granier, 1992; Charlson et al., 2001).

Submicron mineral dust particles ejected by volcanoes and other natural processes also act as condensation nuclei and are effective nuclei for ice formation and intense precipitation (Koop, 2000; Ramanathan et al., 2001; Graf, 2004). Electrostatic forces and the adsorption and condensation of gases onto ash particles produce aggregation of particulates into near-millimeter size clusters or into the so-called accretionary lapilli that readily fall out from the eruption column (Sheridan and Wohletz, 1983; Rose et al., 1995; Schumacher and Schmincke, 1995). Fig. 7.1 summarizes some possible volcanic plume pathway processes pertaining to gas–gas, particulate–particulate, and gas–particulate interactions.

The amounts of gases and volatiles ejected into the atmosphere depend on the total eruption rate and magma composition. El Chichón in Mexico in 1982 and Mount Pinatubo in the Philippines in 1991 each discharged several cubic kilometers of material and released large quantities of SO_2 and HCl into the atmosphere. Pinatubo, for example, released some 20 Mt of SO_2 and 4.5 Mt of HCl (Westrich and Gerlach, 1992, quoted in Tabazadeh and Turco, 1993).

Sulfur compounds react with water vapor and produce sulfate aerosols in the stratosphere, where they scatter light and may produce global scale weather changes (Luhr, 1991; Robock, 2000; Blake, 2003; Scaillet et al., 2003). Hydrogen halides HCl and HBr are highly soluble in liquid water and are, therefore, principally scavenged in the troposphere by the condensed water vapor (Tabazadeh and Turco, 1993), but, in eruptions with little water, significant quantities can reach the stratosphere where they can reduce the stratospheric ozone (Textor et al., 2003). SO_2 and H_2S are only slightly soluble in water and easily reach the stratosphere. Precipitation and wet ash particulates thus remove SO_2, HCl, HF, and other volcanic gases in one part of the atmosphere and may re-introduce these gases in another part where the water evaporates. The large sulfuric acid particles typically contain volcanic ash particles (Pueschel and Russell, 1994). Condensing water vapor releases the latent heat and causes the plume to ascend even higher (Glaze et al.,

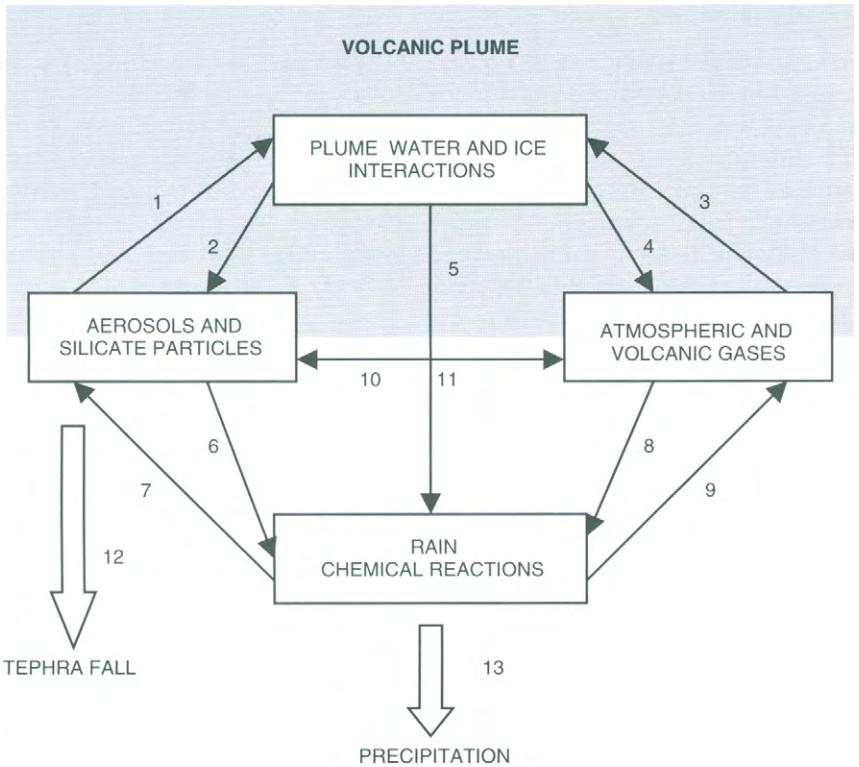

Fig. 7.1. Illustration of possible interaction pathways in a volcanic plume consisting of aerosols and silicate particles; water vapor, water droplets, and ice crystals; atmospheric and volcanic gases; and raindrops. 1: Aerosols/particulates–plume (nucleation scavenging); 2: Plume–aerosols/particulates (condensation/sublimation of water vapor); 3: Gases–plume (dissolution reactions); 4: Plume–gases (evaporation); 5: Plume–rain reactions, 6: Aerosols/particulates–rain (aggregation); 7: Rain–aerosols/particulates (evaporation); 8: Gases–rain (below plume scavenging); 9: Rain–gases (evaporation); 10: Gases–aerosols/particulates adsorption reactions, 11: Aerosols/particulates–gases reactions; 12: Tephra fall; and 13: Precipitation.

1997), while the evaporation of water and melting of ice cause the plume to loose energy. The energy in the plume is thus distributed between different layers of the atmosphere and this distribution changes during an eruption. Moreover, large size particles generally require longer times than small particles to transfer volatile compounds between the particulate and gaseous phases (Meng and Seinfeld, 1996).

Condensed forms of metallic and non-metallic elements and compounds, aqueous solution droplets, solid ash and ice particles, and mixed acid/ash particles contribute to the aerosol and particulate budgets of volcanic clouds, and together with volcanic (and air pollution) gaseous species interact to produce complex dispersion characteristics of explosive eruptions. Micron and submicron size particles can be particularly dangerous to human lungs, especially when combined with acids and other organic and inorganic species (Murphy, 2005).

7.2.2. Plume turbulence

The characteristics of a volcanic plume are determined by the thrusting effect of the material being discharged from the volcanic vent and by the buoyancy of the warm, wet plume ascending into an atmosphere that is drier and subjected to local weather conditions. As a result, the plume is highly heterogenous in terms of thermodynamics and microphysics, and this is reflected in the coupling of turbulence processes at different scales.

The entrainment–mixing processes reduce the plume buoyancy and contribute to the vertical and lateral redistributions of heat, water vapor, and particulate matter. Turbulence is produced from large-scale mean flow instabilities and dissipated at centimeter scales and below where it interacts with particles because of their inertia and causes particulate number or loading ratio fluctuations that affect aggregation, fragmentation, and condensation/evaporation processes.

Let us represent by u and v typical velocities associated with the largest and smallest eddies, respectively, and by ℓ and η the length scales of the largest (integral scale) and smallest eddy structures. From experiments, it is known that the eddies break up on a timescale associated with their turn-over time, and so, on the average, the energy produced by the largest eddies (u^3/ℓ) is dissipated by the smallest ones because of their high velocity gradients ($\varepsilon \sim \nu(v/\eta)^2$). We thus have

$$\varepsilon \sim \frac{u^3}{\ell} \sim \nu\left(\frac{v}{\eta}\right)^2 \tag{7.1}$$

where ν is the kinematic viscosity of the fluid and ε is the energy dissipation rate.

The large-scale mean flow is driven by inertia and buoyancy forces, and this flow continuously cascades energy down to the smallest eddies. This cascade is halted when the Reynolds number, based on small eddy size, is of order unity, that is $v\eta/\nu \sim 1$. Combining these expressions and defining

$$\mathrm{Re}_t = \frac{u\ell}{\nu} \tag{7.2}$$

as the large-scale eddy turbulent Reynolds number, we obtain the following expressions for Re_t and Kolmogorov microscales η and v

$$\mathrm{Re}_t \sim \frac{u^4}{\varepsilon\nu}, \quad \eta \sim \left(\frac{\nu^3}{\varepsilon}\right)^{1/4}, \quad v \sim (\nu\varepsilon)^{1/4} \tag{7.3}$$

For typical volcanic plumes, $u \sim 10\,\mathrm{ms}^{-1}$, $\ell \sim 10^2\,\mathrm{m}$, $\nu = 10^{-5}\,\mathrm{m^2s^{-1}}$, and thus $\varepsilon \sim 10^{-2}\,\mathrm{m^2s^{-3}}$, $\eta \sim 1\,\mathrm{mm}$, $v \sim 1\,\mathrm{cm\ s^{-1}}$, and $\mathrm{Re}_t = 10^8$. This means that both atmospheric clouds and volcanic plumes have very large Reynolds numbers, which implies that much of the total turbulence-produced Reynolds stress lies in the small scales (Ferziger, 1993) where the energy is dissipated and coupled with local microphysical processes. The small-scale turbulence is thus inherently linked to the large-scale turbulent characteristics of the plume and this coupling produces anisotropy at small scales and fluctuations of passive scalars advected by this turbulence (Sreenivasan and Antonia, 1997; Warshaft, 2000). This intermittency, or probability of large–amplitude

fluctuations, appears to be associated with the vortex stretching, which 'teases out the vorticity into finer and finer filaments' (Davidson, 2004, p. 378). Local plume temperature, humidity, particulate concentration, and other flow properties can thus fluctuate with significant amplitudes, and there is a growing consensus that both the collision rate and the collision efficiency of particles increase with turbulence–particle interactions at centimeter scales and below, including clustering of particles in regions of low vorticity or high strain rate owing to their finite inertia (Shaw, 2003). The microphysical processes in volcanic plumes thus depend on the properties of the turbulent flow in which the droplets and other particles reside; these processes, in turn, modify both the turbulent energy dissipation at small scales and the turbulence generation by inertia and buoyancy at integral scales. For particle volumetric fractions less than about 10^{-6}, the particles have a negligible effect on gas turbulence, but, at larger fractions, they begin to modulate the gas turbulence, so that large particles lead to turbulent energy production and small particles to turbulent energy dissipation. When the particle volumetric fraction exceeds about 10^{-3}, particle–particle collisions take place and a two-way coupling between the gas and particle turbulence is expected (Crowe, 1982).

The turbulent flow of particulates in a volcanic plume is governed by several forces which define the non-dissipative and dissipative characteristic response times of different processes. The *convective time* is defined by equating the non-steady inertia and convective inertia forces, the *settling time* by equating the non-steady inertia and buoyancy forces, the *thrusting time* by equating the convective inertia and pressure forces, and the *surface tension time* by equating the non-steady inertia and surface tension forces. We also have the characteristic times associated with particle rotation, collision, and dilatancy. In addition, we have the dissipative times associated with momentum, heat, and mass diffusion. These times have different values in different regions of the plume (near the vent, in the jet thrust region, in the convective region where buoyancy is important, in pyroclastic flows close to the ground) and thus no simple model or scaling of pyroclastic dispersions can be used for our modeling objectives.

Particles with very small Stokes number (ratio of non-steady inertia to momentum diffusion times) readily respond to turbulent fluctuations, while those with very high Stokes numbers tend to move quite independently of the surrounding fluid. In the intermediate range of Stokes numbers, the particles tend to produce *inertial clustering*, or move out of the regions of high vorticity and congregate into regions of high strain (Dobran and Hur, 1990; Eaton and Fessler, 1994; Reade and Collins, 2000; Wang et al., 2000).

Since the small eddies of volcanic plumes have millimeter-size structures, the prospects for direct numerical simulation (DNS) of such structures are not foreseable in the near future, because such simulations should also resolve large eddies for tens and hundreds of kilometers around the volcanic vent. Despite of the present unwieldiness of DNS, we cannot ignore the smallest eddies in the flow because they dissipate the energy being produced by the large eddies and thus affect these structures. This implies that we must reliably model the effects of the small-scale flow without requiring the resolution of every detail of the tiniest eddy structures.

In Reynolds-averaged models, only the mean flow is computed and the *turbulence closure* is provided through eddy diffusivity or one or more transport equations that account for the generation and dissipation of turbulence. In large eddy simulation (LES) models, the smallest scales are averaged out while the large scales are computed directly. This essentially assumes that small eddies in a flow are more isotropic than large ones and that they can be universally modeled through some suitable scale invariance algebraic models (Smagorinsky, 1993; Meneveau and Katz, 2000; Wagner and Liu, 2000). The discretization for LES is, in general, much finer and more accurate and physically correct than that involved in Reynolds-averaged models.

Multiphase flow models based on ensemble or time averaging are too complicated and poorly constrained by the large number of modeling parameters (Elghobashi and Abou-Arab, 1983; Ahmadi and Ma, 1990), and have limited practical utility for more than two phases. The eddy viscosity gas phase turbulence models of Valentine and Wohletz (1989) and Dobran et al. (1993) (and subsequent variants of this model as in Dartevelle, 2004; Ongaro et al., 2004) suffer from the major flaw of not accounting properly for interphase turbulence coupling, and convection and diffusion of turbulence. The turbulent fluctuations at a point depend in part on the global structure of the flow, and on how these fluctuations are dissipated at small scales affects their generation at large scales. As noted above, there is a strong coupling between turbulence and particulates of different sizes, and any volcanic plume model that does a poor job of accounting for such a coupling should not be employed for predictive simulations of volcanic eruptions. Due to their physical and numerical modeling deficiencies, the current pyroclastic dispersion models are unsuitable for use in a Global Volcanic Simulator.

7.2.3. Particulate distributions

Walker (1981) classified explosive volcanic eruptions according to their dispersal and fragmentation indices. The *dispersal index* (D) measures the area over which the pyroclastic deposit is dispersed and is correlated in terms of the eruption column height, whereas the *fragmentation index* (F) measures the degree of fragmentation of the pyroclastic material and is correlated in terms of the rheology of the erupted material. High F's produce highly fragmented magmas and copious amounts of small particulates with grain sizes corresponding to fine ash (less than 63 μm or $\phi 4$, $\phi = -\log_2 d_{grain}$, with d_{grain} being in mm). Plinian eruptions produce 30 km high or even higher eruption columns where as much as 25% of the material emitted is fine ash and dust and 50% is of sub-millimeter size. Ultraplinian eruptions (such as Taupo, ca. 186, New Zealand) produce over 80% of particulates of sub-millimeter range and the eruption cloud rises high into the stratosphere (20–50 km above the surface of the Earth). Ignimbrite-forming eruptions produce pyroclastic flows and normally follow the initial plinian phase. Fine ash content of ignimbrites varies significantly, from 15% to 85%, and many ignimbrites appear to consist of sub-millimeter particles (Giordano and Dobran, 1994).

Both post-eruption fragmentation and co-ignimbritic ash settling mechanisms operate in producing such deposits. Phreatoplinian eruptions can also produce

30–40% of fine ash, and as much as 1–4% of ash that is finer than 4 μm. These ash clouds are especially prone to scavenging by water, and raining often takes place. Wet particulates tend to stick together and produce millimeter-size particles which together with rain droplets and coarse blocks (particles greater than 64 mm) fall early from the eruption column along ballistic or near-ballistic trajectories. The amounts of very fine particulates emitted from volcanoes are currently poorly constrained, because of the practical lower limit of dry sieving (which is about 4 μm or $\phi 8$) and lack of suitable instruments to resolve particles with different physical and chemical properties (NCAR, 2000).

The particulates in volcanic deposits tend to follow the log–normal distribution (Walker, 1981), with large explosive eruptions producing larger sizes than the waning stages of phreatomagmatic activity (Hobbs et al., 1982). The very fine atmospheric aerosols and particulates associated with nuclei (0.005–0.01 μm) and accumulation (0.1–2.5 μm) modes also appear to follow this distribution (Seinfeld and Pandis, 1998).

The nuclei mode aerosols form from the condensation of vapors and nucleation of atmospheric and volcanic species. They are lost primarily by coagulation with larger particles. The accumulation mode particles form from the aggregation of particles in the nuclei mode and condensation of vapors onto existing particles. These particles grow into cloud condensation nuclei and wash out from eruption clouds. Particles of diameters greater than 2.5 μm have sufficiently large sedimentation velocities and their temporal and spatial distributions in a volcanic plume depend on the heat, mass, and momentum characteristics of the gaseous environment.

The particulate distribution spectrum of a volcanic plume can be modeled by a multimodal particle distribution function which has the general shape illustrated in Fig. 7.2, with its detailed spectrum changing temporarily and spatially, depending on the microphysical processes in the plume and the changing character of the volcanic material emitted from the volcano. Gas–particulate interactions in the plume produce, at least, a dozen different processes which include particulate fragmentation and agglomeration, evaporation and condensation, and chemical reactions (Fig. 7.1). These processes depend, in turn, on the conditions of pyroclasts exiting from the vent and on the dynamic and thermal conditions of the atmosphere into which the volcanic products are being discharged. The conditions of pyroclasts at the vent depend, in turn, on the characteristics of the ascending magma and on the vent geometry, which change due to the conduit erosion processes. A useful pyroclastic dispersion model should, therefore, include or be coupled with other models that account for such processes.

As a first approximation, the particle distribution function in Fig. 7.2 can be patched by several log–normal or other suitable distributions, but such an approach is not very useful for our purposes. What needs to be done is to determine dynamically the temporal and spatial variation of particulate size as a result of condensation, evaporation, aggregation, fragmentation, and mass transfer processes, and thus ascertain the dispersion and fall-out characteristics of pyroclastic material during an eruption. If a particle is chosen at random from a volume containing many particles, $p(r)$ is the probability of choosing such a particle with the radius

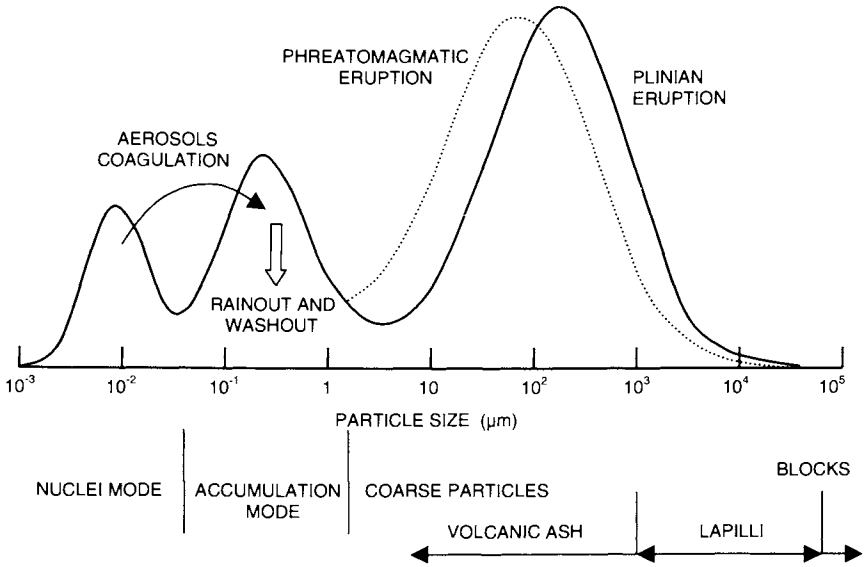

Fig. 7.2. Particulate distributions in nuclei mode, accumulation mode, and coarse particle mode. The coarse particle mode includes coarse ash, raindrops, lapilli, and blocks. The ultraplinian and phreatomagmatic eruptions shift the coarse particle distribution toward finer particles. Aerosols aggregate to form cloud condensation nuclei and together with fine ash can fall from the eruption column in the form of dry and/or wet particulate matter.

between r and $r+dr$. We thus have $\int_0^\infty p(r)dr = 1$, with $f(r) = np(r)$ being the number of particles of radius r per unit volume and n the number of particles of all sizes in this volume. f has both spatial and temporal dependence, and can assume a complicated form if we include the thermodynamic phase and chemical composition of particles into its description. If, in a first approximation, we ignore these complications and extend the dynamic equation for particle size distribution of Gelbard and Seinfeld (1979) to the situation where f depends explicitly on time, particle size, and position within the plume, we obtain

$$\frac{\partial f(r,\mathbf{x},t)}{\partial t} + \frac{\partial \dot{r} f(r,\mathbf{x},t)}{\partial r} + \frac{\partial v_{pj} f(r,\mathbf{x},t)}{\partial x_j} = J + S - R$$
$$+ \frac{1}{2}\int_0^r \left(1 - \frac{r'^3}{r^3}\right)^{-2/3} \kappa((r^3 - r'^3)^{1/3}, r', \mathbf{x}) f((r^3 - r'^3)^{1/3}, \mathbf{x}, t)$$
$$\times f(r', \mathbf{x}, t)\, dr' + \int_0^\infty \kappa(r, r', \mathbf{x})(1+\eta) f(r, \mathbf{x}, t) f(r', \mathbf{x}, t)\, dr' \qquad (7.4)$$

where we have included the effect of particle correlations in the collision integral.

In this Boltzmann-like transport equation, the first term on the left of the equation accounts for the increase in the number of particles and the second term for the growth from condensation and evaporation ($\dot{r}\,\partial f/\partial t$) and change in the distribution of f from these processes ($f\partial \dot{r}/\partial t$). The third term accounts for the change in f at different spatial locations. The fifth term on the right of the equation

accounts for collisions and the fourth term for coalescence or aggregation of particles. J is the nucleation rate, S is the source rate, and R is the sink rate of particles. κ is the collision kernel and η is the pair correlation function. In atmospheric clouds, the particle growth is normally dominated by condensation in the earliest stages of cloud development when the droplets are small, and, as the droplets grow, this process is dominated by particle collisions and coalescence. Some collision and coalescence kernels are available in Pruppacher and Klett (1997) and Seinfeld and Pandis (1998), but these need to be modified for applications to volcanic plumes. Equation (7.4) must be coupled with mass, momentum, and energy transport equations to determine the evolution of particle distribution in space and time.

The particulate distribution in Fig. 7.2 can be divided into $m+n$ disperse phases, where all particles smaller than a certain size belong to the set m and the others belong to the set n. This division can be decided on the basis of the parameter $\mathscr{F}$, which is defined as follows

$$(1-\mathscr{F})\bar{d}_c \leqslant d_c \leqslant \bar{d}_c(1+\mathscr{F}), \quad c=1,\ldots,m+n \tag{7.5}$$

By this rule, the number of particle cluster groups c is dynamic, because no particle belonging to cluster c is allowed to exceed or fall below the mean particle size $\bar{d}_c$ of that cluster of particles by the fraction $\mathscr{F}$. This parameter is optimized through verification and validation procedures. The atmospheric and volcanic gases and vapors can be included into one phase consisting of several components, such as N_2, O_2, H_2O vapor, CO_2, CO, SO_2, and HCl. Water in liquid (droplets) and solid (ice) states can include the dissolved inorganic and organic compounds (Pilinis and Seinfeld, 1988; Dominé and Thibert, 1996) and belongs to the disperse phases. Coarse particles of raindrops, pumices, lapilli, and lithic blocks in the particulate spectrum of Fig. 7.2 belong to the set n.

An arbitrary macroscopic region of the atmosphere into which volcanic products are being emitted can thus be modeled with $m+n+1$ phases, where each phase may consist of one or more chemical components undergoing chemical reactions. The number of phases in such a region changes because of particulate nucleation, fragmentation and aggregation, evaporation and condensation of volatiles, and chemical reactions among the phase constituents.

For m clusters of fine particulates and gas phase, we can employ the Eulerian formulation framework of physical laws, whereas for the n coarse particulate clusters we can use the Lagrangian framework. This choice is particularly effective in our situation because of both the very large number of fine particulates which tend to follow the turbulent dispersion of the gas phase and the significant number of coarse particles which poorly interact with the gas medium and fine particulates and tend to follow near-ballistic trajectories.

7.2.4. Eulerian form of material transport laws

The physical laws governing the transport of mass, momentum, and energy of $m+1$ Eulerian phases can be established through formal averaging procedures

involving the well-established single-phase macroscopic transport model of matter (Ishii, 1975; Dobran, 1991; Drew and Passman, 1999). The averaging procedure acts like a filter that eliminates detailed tracking of particles while allowing for their gross motions and interactions. From among these averaging procedures, the volume averaging is most useful, for it not only furnishes the desired mass, momentum, energy, and entropy transport laws for each phase of a multiphase mixture, but it also provides an additional set of transport equations which account for the structural properties of the mixture (Dobran, 1991, 1992). These averaged transport equations account for the size of the averaging region and thus recover some of the lost information involved in the averaging process.

A structural model of multiphase mixtures eliminates the complications associated with turbulence modeling based on the Reynolds-averaging procedures of single-phase flows and parallels that of LES where only the local turbulence scales are averaged while the large scales are computed.

Structural properties of multiphase mixture include particle inertia, rotation, and dilatancy (expansion–contraction effects), and can be directly associated with turbulence production and dissipation. The structural effects of multiphase mixtures are intimately tied with the microphysical processes at the centimeter and smaller scales where the turbulent energy is dissipated and thus contribute to the global plume dynamics where this energy is produced.

All current pyroclastic dispersion models do not account for a systematic coupling between different turbulence scales and, therefore, fail short in their predictive capabilities for modeling long-duration and high-rising volcanic plumes. As discussed above, turbulence is ubiquitous in volcanic plumes and no serious attention has been paid to date to the effects of large turbulence Reynolds numbers on energy dissipation, coupling between small and large scales of turbulence, effects of Stokes number or particle size, particle loading, volume fraction, particle settling parameter, and other ratios of viscous, inertia, and buoyancy forces.

In the structured model of multiphase mixtures developed by Dobran (1991, 2001), a macroscopic averaging volume U contains all phases of the mixture and the local thermodynamic properties F^α of phase α appear as *volume-averaged* variables

$$\langle F^\alpha \rangle = \frac{1}{U_\alpha} \int_{U_\alpha} F^\alpha \, dU \tag{7.6}$$

where U_α is the volume of phase α in U.

The *density-weighted average* F_α, *partial average* $\bar{F}_\alpha$, and *phase average* $\bar{\bar{F}}_\alpha$ are defined as

$$F_\alpha = \frac{\langle \rho^\alpha F^\alpha \rangle}{\langle \rho^\alpha \rangle} = \frac{1}{\bar{\rho}_\alpha} \frac{U_\alpha}{U} \langle \rho^\alpha F^\alpha \rangle \tag{7.7}$$

$$\bar{F}_\alpha = \frac{U_\alpha}{U} \langle F^\alpha \rangle, \quad \bar{\bar{F}}_\alpha = \langle F^\alpha \rangle \tag{7.8}$$

The *partial density of phase* α denotes the mass of phase α per unit volume of the mixture and is defined by

$$\bar{\rho}_\alpha = \frac{U_\alpha}{U}\langle \rho^\alpha \rangle = \phi_\alpha \bar{\bar{\rho}}_\alpha \tag{7.9}$$

where ϕ_α is the *volume fraction* (U_α/U) and $\bar{\bar{\rho}}_\alpha$ is the volume-averaged mass density of phase α in the averaging volume.

The *density of the multiphase mixture* is obtained by summing the partial densities over all the phases

$$\bar{\rho} = \sum_{\alpha=1}^{\gamma} \bar{\rho}_\alpha \tag{7.10}$$

whereas the *velocity of phase* α, $\mathbf{v}_\alpha$, and the *mixture velocity*, $\mathbf{v}$, are defined as

$$\mathbf{v}_\alpha = \frac{1}{\bar{\rho}_\alpha}\frac{U_\alpha}{U}\langle \rho^\alpha \mathbf{v}^\alpha \rangle, \quad \mathbf{v} = \frac{1}{\bar{\rho}}\sum_{\alpha=1}^{\gamma} \bar{\rho}_\alpha \mathbf{v}_\alpha \tag{7.11}$$

The *diffusion velocity* of phase α, $\mathbf{u}_\alpha$, is the velocity relative to the center of mass and satisfies

$$\mathbf{u}_\alpha = \mathbf{v}_\alpha - \mathbf{v}, \quad \sum_{\alpha=1}^{\gamma} \bar{\rho}_\alpha \mathbf{u}_\alpha = 0 \tag{7.12}$$

The backward prime affixed to a phase variable denotes the *material derivative* following that phase.

By employing the above definitions, the averaging procedure produces the following expression for the *balance of mass of phase* α

$$\dot{\bar{\rho}}_\alpha + \bar{\rho}_\alpha \nabla \cdot \mathbf{v}_\alpha = \hat{c}_\alpha \tag{7.13}$$

where the mass generation rate per unit volume of the mixture $\hat{c}_\alpha$ arises from the phase change processes

$$\hat{c}_\alpha = -\frac{1}{U}\int_{a^\wedge} m^\alpha \, da \tag{7.14}$$

where $a^\wedge$ denotes the interfacial area of phase α in U and m^α is the local mass transfer rate across the interface. $\hat{c}_\alpha$ is equal to zero if there is no mass transfer across the interfaces.

The conservation of mass for a multiphase mixture is obtained by summing from $\alpha = 1$ to $\alpha = \gamma$ in Equation (7.13). This produces

$$\frac{\partial \bar{\rho}}{\partial t} + \nabla \cdot \bar{\rho}\mathbf{v} = 0 \quad \text{or} \quad \dot{\bar{\rho}} + \bar{\rho}\nabla \cdot \mathbf{v} = 0 \tag{7.15}$$

where use was made of the mass conservation property of the mixture

$$\sum_{\alpha=1}^{\gamma} \hat{c}_\alpha = 0 \tag{7.16}$$

In Equation (7.15) the dot over the mixture density signifies the *material derivative* following the motion of the mixture as a whole.

The *linear momentum of phase* α is expressed by

$$\bar{\rho}_\alpha \dot{\mathbf{v}}_\alpha = \nabla \cdot \bar{\mathbf{T}}_\alpha + \bar{\rho}_\alpha \mathbf{b}_\alpha + \hat{\mathbf{p}}_\alpha \tag{7.17}$$

where $\bar{\mathbf{T}}_\alpha$ is the stress tensor and $\mathbf{b}_\alpha$ is the body force per unit mass. $\hat{\mathbf{p}}_\alpha$ is the momentum source per unit volume and arises from phase changes and structural effects of the mixture because of the finite size of the averaging volume U.

The *angular momentum of phase* α expresses the non-symmetry of the stress tensor

$$\mathbf{M}_\alpha = \bar{\mathbf{T}}_\alpha - \bar{\mathbf{T}}_\alpha^T \tag{7.18}$$

where the superscript T denotes transpose. This asymmetry can be produced by particle spins, couple stresses, and body moments.

The *conservation of energy of phase* α takes the following form

$$\bar{\rho}_\alpha \dot{\varepsilon}_\alpha = \mathrm{tr}(\bar{\mathbf{T}}_\alpha^T \cdot (\nabla \mathbf{v}_\alpha)) - \nabla \cdot \bar{\mathbf{q}}_\alpha + \bar{\rho}_\alpha r_\alpha + \hat{\varepsilon}_\alpha \tag{7.19}$$

where ε_α is the internal energy, tr denotes the trace operation, $\bar{\mathbf{q}}_\alpha$ is the heat flux vector, r_α is the energy generation rate per unit mass, and $\hat{\varepsilon}_\alpha$ accounts for both the energy transfer rate per unit volume between the phases and the structural properties of the mixture.

The *entropy inequality of phase* α satisfies

$$\bar{\rho}_\alpha \dot{s}_\alpha + \nabla \cdot \left(\frac{\bar{\mathbf{q}}_\alpha}{\bar{\bar{\theta}}_\alpha} \right) - \frac{\bar{\rho}_\alpha r_\alpha}{\bar{\bar{\theta}}_\alpha} + \hat{c}_\alpha s_\alpha + \hat{s}_\alpha \geqslant 0 \tag{7.20}$$

where s_α is the entropy, $\bar{\bar{\theta}}_\alpha$ is the *phase averaged temperature*, and $\hat{s}_\alpha$ is the *entropy source of phase* α that is not necessarily positive semi-definite.

The phasic conservation of mass, linear momentum, energy, and entropy Equations (7.13) (7.17–7.20) are similar to the corresponding equations of single-phase multicomponent mixtures and reduce to the latter if the interfacial effects of the mixture are negligible. Every physically consistent theory of multiphase mixtures should have such a *consistency property* in order to reproduce, at least, the most simple and known physical phenomena.

The motion of each phase relative to the center of mass is accounted for by taking moments of the phasic conservation of mass and momentum equations *relative to the center of mass*. These operations produce the *balance of equilibrated inertia*

$$\bar{\rho}_\alpha \dot{i}_\alpha = -\hat{c}_\alpha (i_\alpha - \hat{i}_\alpha) + 2\bar{\rho}_\alpha i_\alpha \frac{\dot{\phi}_\alpha}{\phi_\alpha} - \nabla \cdot \left(\mathbf{U}_\alpha \frac{\dot{\phi}_\alpha}{\phi_\alpha} \right) \tag{7.21}$$

and *balance of equilibrated moments*

$$\overline{\rho_\alpha i_\alpha \frac{\dot{\phi}_\alpha}{\phi_\alpha}} = -\hat{c}_\alpha \frac{\dot{\phi}_\alpha}{\phi_\alpha}(i_\alpha - \hat{i}_\alpha) + \bar{S}_\alpha + \nabla \cdot \bar{\boldsymbol{\lambda}}_\alpha - \bar{\rho}_\alpha i_\alpha \frac{\dot{\phi}_\alpha}{\phi_\alpha} \nabla \cdot \mathbf{v}_\alpha + \bar{\rho}_\alpha i_\alpha \left(\frac{\dot{\phi}_\alpha}{\phi_\alpha}\right)^2 - \left(\frac{\dot{\phi}_\alpha}{\phi_\alpha}\right) \nabla \cdot \left(\mathbf{U}_\alpha \frac{\dot{\phi}_\alpha}{\phi_\alpha}\right) \tag{7.22}$$

where the *isotropic inertia of phase* α is defined as

$$i_\alpha = \frac{1}{\bar{\rho}_\alpha} \frac{1}{U} \int_{U_\alpha} \rho^\alpha \boldsymbol{\xi} \cdot \boldsymbol{\xi} \, dU \tag{7.23}$$

with $\boldsymbol{\xi}$ being the position vector relative to the center of mass. In the equilibrated inertia equation, $\hat{i}_\alpha$ represents the source of inertia due to phase change, whereas $\mathbf{U}_\alpha$ accounts for triple correlations of $\boldsymbol{\xi}$ which are associated with the nonuniformities within the averaging volume. The moment of surface forces acting on the surface of volume U_α in U is represented in the equilibrated moments equation by $\bar{S}_\alpha$, whereas $\bar{\boldsymbol{\lambda}}_\alpha$ in this expression represents the volume-averaged moment of the stress tensor $\bar{\mathbf{T}}_\alpha$.

The above multiphase field equations are the result of replacing continuous distribution of forces in the averaging volume by the resultant forces and couples acting on this volume. When the forces acting on the surface of U_α are averaged, the result is an average force which is represented by the surface traction force $\bar{\mathbf{T}}_\alpha \cdot \mathbf{n}_\alpha$ and a resultant couple represented by $\bar{\mathbf{S}}_\alpha$. Similarly, the average stress tensor $\bar{\mathbf{T}}_\alpha$ and intrinsic stress moment $\bar{\boldsymbol{\lambda}}_\alpha$ replace the local variation of stress tensor within U_α. These results are, therefore, consistent with particle mechanics where the forces acting on a collection of particles can be replaced by a resultant force and a resultant couple. The structural properties of the mixture are thus accounted for by i_α, $\mathbf{U}_\alpha$, $\bar{\mathbf{S}}_\alpha$, and $\bar{\boldsymbol{\lambda}}_\alpha$, and may also appear in the phasic variables $\bar{\mathbf{T}}_\alpha$, $\hat{\mathbf{p}}_\alpha$, $\bar{\mathbf{q}}_\alpha$, $\hat{i}_\alpha$, $\hat{\varepsilon}_\alpha$, and $\hat{c}_\alpha$. These variables are required to satisfy certain constitutive principles and the second law of thermodynamics as represented by Equation (7.20).

When some of the results of constitutive theory of mixtures of fluids (Dobran, 1991) are used in the above transport equations, these expressions, expressed in the tensor index notation with indices i, j, and k, reduce to the following forms:

Conservation of mass:

$$\frac{\partial \bar{\rho}_\alpha}{\partial t} + \frac{\partial \bar{\rho}_\alpha v_{\alpha j}}{\partial x_j} = \hat{c}_\alpha, \quad \bar{\rho}_\alpha = \phi_\alpha \bar{\bar{\rho}}_\alpha \tag{7.24}$$

$$\frac{\partial \bar{\bar{\rho}}_\alpha}{\partial t} + \frac{\partial \bar{\bar{\rho}}_\alpha v_{\alpha j}}{\partial x_j} = \frac{\hat{c}_\alpha}{\phi_\alpha} - \bar{\bar{\rho}}_\alpha \varphi_\alpha, \quad \varphi_\alpha = \frac{\dot{\phi}_\alpha}{\phi_\alpha} \tag{7.25}$$

Conservation of momentum:

$$\frac{\partial \bar{\rho}_\alpha v_{\alpha i}}{\partial t} + \frac{\partial \bar{\rho}_\alpha v_{\alpha i} v_{\alpha j}}{\partial x_j} = -\phi_\alpha p_{\alpha,i} - \frac{1}{2}\bar{\rho}_\alpha i_\alpha (\varphi_\alpha^2)_{,i} + (O_{\alpha\alpha}\phi_\alpha \varphi_\alpha)_{,i} + \hat{c}_\alpha v_{\alpha i} + [\lambda_{\alpha\alpha} D_{\alpha kk}\delta_{ij} + 2\mu_{\alpha\alpha} D_{\alpha ij} + 2\bar{\rho}_\alpha C_\alpha \phi_{\alpha,i}\phi_{\alpha,j}]_{,j} - \sum_{\beta}^{\gamma-1} \xi_{\alpha\beta}(v_{\beta i} - v_{\gamma i}) - \sum_{\beta}^{\gamma} \gamma_{\alpha\beta}\bar{\bar{\theta}}_{\beta,i} - \sum_{\beta}^{\gamma} \Delta_{\alpha\beta}\bar{\bar{\rho}}_{\beta,i} + \bar{\rho}_\alpha b_{\alpha i} \quad (7.26)$$

where $D_{\alpha ij}$ is the deformation rate tensor and an index following a comma in a subscripted variable denotes the partial derivative with respect to that index; for example, $p_{\alpha,i} = \partial p_\alpha / \partial x_i$. In Equation (7.26), p_α is the thermodynamic pressure, $\lambda_{\alpha\alpha}$ and $\mu_{\alpha\alpha}$ are the bulk and shear viscosity coefficients, respectively, C_α and $O_{\alpha\alpha}$ are structural property coefficients, $\xi_{\alpha\beta}$ are viscous drag coefficients, $\gamma_{\alpha\beta}$ are Soret effect coefficients, and $\Delta_{\alpha\beta}$ are density gradient coefficients. The viscosity coefficients include both viscous and turbulent contributions and the latter can be modeled on the basis of the subgrid scale model of Smagorinsky (1993) or some other more refined approaches. The stress term with the parameter C_α accounts for Mohr–Coulomb yield-type criteria for plastic deformation when the volume fraction gradients become high and the flow begins to creep as in pyroclastic flows during material sedimentation. In this situation, the pressure gradient becomes balanced by the gravity and compaction characteristics of particulates. This stress term thus accounts for the yield stress of the material and is independent of the rate of strain. It produces energy dissipation (see Equation (7.28) below).

Conservation of total energy:

One can derive several useful forms for the energy equation. The one that we will need is the total energy equation which is obtained by adding the scalar product of velocity and momentum Equation (7.17) to the internal energy Equation (7.19). With the total energy being defined as the sum of internal, kinetic, and compaction energies

$$e_\alpha = \varepsilon_\alpha + \frac{1}{2} v_{\alpha i} v_{\alpha i} + C_\alpha \phi_{\alpha,i}\phi_{\alpha,i} \quad (7.27)$$

the result of these operations can be expressed as follows:

$$\frac{\partial \bar{\rho}_\alpha e_\alpha}{\partial t} + \frac{\partial \bar{\rho}_\alpha e_\alpha v_{\alpha j}}{\partial x_j} = -\bar{q}_{\alpha i,i} - \phi_\alpha (p_\alpha v_{\alpha i})_{,i} + (O_{\alpha\alpha}\phi_\alpha \varphi_\alpha v_{\alpha i})_{,i} + [(\lambda_{\alpha\alpha} D_{\alpha kk}\delta_{ij} + 2\mu_{\alpha\alpha} D_{\alpha ij} + 2\bar{\rho}_\alpha C_\alpha \phi_{\alpha,i}\phi_{\alpha,j}) v_{\alpha i}]_{,j} - v_{\alpha i} \sum_{\beta}^{\gamma-1} \xi_{\alpha\beta}(v_{\beta i} - v_{\gamma i}) - v_{\alpha i} \sum_{\beta}^{\gamma} \gamma_{\alpha\beta}\bar{\bar{\theta}}_{\beta,i} - v_{\alpha i} \sum_{\beta}^{\gamma} \Delta_{\alpha\beta}\bar{\bar{\rho}}_{\beta,i} + \bar{\rho}_\alpha b_{\alpha i} v_{\alpha i} + \bar{\rho}_\alpha r_\alpha - \bar{q}_{s\alpha} + \hat{c}_\alpha \left(\hat{\hat{\varepsilon}}_\alpha + \frac{1}{2} v_{\alpha i} v_{\alpha i} + C_\alpha \phi_{\alpha,i}\phi_{\alpha,i} \right) - \phi_\alpha \varphi_\alpha (p_\alpha - \beta_\alpha) - v_{\alpha i} \frac{1}{2} (\varphi_\alpha^2)_{,i} \bar{\rho}_\alpha i_\alpha \quad (7.28)$$

In this equation $\bar{q}_{s\alpha}$ is the interfacial heat transfer rate per unit volume, whereas the *configuration pressure* β_α (Goodman and Cowin, 1972; Passman et al., 1984) is computed from the Helmholtz potential

$$\beta_\alpha = \bar{\rho}_\alpha \frac{\partial \psi_\alpha}{\partial \phi_\alpha} \tag{7.29}$$

This pressure arises from the changes in the packing of phase α and thus reflects the strength of contact forces between this and other phases. A reasonable choice for this pressure is the packing stress of material grains.

The total energy Equation (7.28) shows how the energy of each phase is distributed between different processes. The convection of energy is balanced by heat transfer due to temperature gradients within the phases, temperature differences between the phases, phase changes releasing or requiring latent heat, viscous dissipation which produces heat from fluid friction within each phase and from the exchange of momenta between the phases, flow work associated with pressure and distribution of phases, energy generation from electromagnetic or other processes, and the work expended in distributing phase matter in different regions of vorticity. The larger the phase inertia and its volume fraction gradient, the more energy from large eddies must be expended or dissipated by the small eddies to maintain equilibrium. The strengths of contact forces between the phases and the phasic dilatation rates can both produce and dissipate energy within a mixture. The redistribution of particulate and non-particulate matter at small scales is thus governed by phase inertia, volume fraction (particle loading), and configuration pressure parameters.

Inertia transport equation:

$$\frac{\partial \bar{\rho}_\alpha i_\alpha}{\partial t} + \frac{\partial \bar{\rho}_\alpha i_\alpha v_{\alpha j}}{\partial x_j} = \hat{c}_\alpha \hat{i}_\alpha + 2\bar{\rho}_\alpha i_\alpha \varphi_\alpha - (\varphi_\alpha U_{\alpha m})_{,m} \tag{7.30}$$

Dilatation–contraction transport equation:

$$\frac{\partial \bar{\rho}_\alpha \varphi_\alpha}{\partial t} + \frac{\partial \bar{\rho}_\alpha \varphi_\alpha v_{\alpha j}}{\partial x_j} = \hat{c}_\alpha \varphi_\alpha - D_{\alpha kk}\left(\bar{\rho}_\alpha \varphi_\alpha + \frac{\phi_\alpha}{i_\alpha} O_{\alpha\alpha}\right) + \frac{1}{i_\alpha} \ddot{\sum_\beta} (K_{\alpha\beta} i_\beta + H_{\alpha\beta} \phi_\beta \varphi_\beta) - \bar{\rho}_\alpha \varphi_\alpha^2 \tag{7.31}$$

The inertia and dilatation–contraction transport equations account for small-scale effects in the flow which have been averaged out through the averaging procedure of local mass, momentum, and energy transport laws. In our model, the microstructural effects survive through phase inertia, volume fraction, and configuration pressure, and provide a feedback to the mean flow. The phase inertia can be viewed as a measure of turbulent intensity and $U_{\alpha m}$ as proportional to the gradient of this intensity.

Since the phase inertia moderates both the production of turbulent kinetic energy and turbulent dissipation rate, the inertia transport Equation (7.30) can be split into two interacting parts that model this turbulence. Such a turbulence model

would then be similar to the one of Darwish et al. (2001), although these authors do not justify the methods used to obtain their model. The size of the averaging volume can be, therefore, interpreted as the filter width, with the microstructural parameters defining its characteristics. The resulting structural model is thus analogous to LES models where the small scales are averaged out and modeled and the large ones are computed. It is also considerably simpler than the multiphase flow turbulence models based on the single-phase flow Reynolds–averaging with too many poorly constrained modeling parameters.

To close the above equations, we also need a constitutive equation for the heat flux rate, which in linearized form can be written as

$$\bar{q}_{\alpha i} = -\sum_{\beta}^{\ddot{\gamma}} \kappa_{\alpha\beta} \bar{\bar{\theta}}_{\beta,i} - \sum_{\beta}^{\ddot{\gamma}} \nu_{\alpha\beta} \bar{\bar{\rho}}_{\beta,i} - \sum_{\beta}^{\ddot{\gamma}-1} \xi_{\alpha\beta}(v_{\beta i} - v_{\ddot{\gamma} i}) - \sum_{\beta}^{\ddot{\gamma}} \Gamma_{\alpha\beta} \phi_{\beta,i} \tag{7.32}$$

where the first term on the right represents the Fourier effect (heat flow due to temperature gradients) and the second term is the Dufour effect (heat flow due to mass transfer). Except for the temperature gradient term in this equation, all other terms can, in general, be neglected. Equation (7.20) places restrictions on the phenomenological coefficients of constitutive equations and requires that the following conditions be satisfied

$$\kappa_{\alpha\alpha} \geq 0; \quad H_{\alpha\alpha} \geq 0; \quad O_{\alpha\alpha} \leq 0; \quad \lambda_{\alpha\alpha} + \frac{2}{3}\mu_{\alpha\alpha} \geq 0;$$
$$\xi_{\alpha\alpha} \geq 0; \quad \xi_{\alpha\beta} \leq 0, \quad \alpha \neq \beta \neq \ddot{\gamma} \tag{7.33}$$

The interfacial heat transfer can be modeled as

$$\bar{q}_{s\alpha} = \bar{h}_{\alpha}(\bar{\bar{\theta}}_{\alpha} - \bar{\bar{\theta}}_{g}) \tag{7.34}$$

where $\bar{\bar{\theta}}_g$ is the temperature of the gas phase and $\bar{h}_\alpha$ is the heat transfer coefficient. The phase change energy flux $\hat{c}_\alpha \hat{\bar{\varepsilon}}_\alpha$ is related to the mass supply $\hat{c}_\alpha$ and average energy of interfaces of phase α. Similarly, the source of inertia $\hat{c}_\alpha \hat{i}_\alpha$ is related to the mass supply and average inertia of interfaces of phase α. Modeling of $\hat{c}_\alpha$ depends on the composition and chemical reactions of the constituents of phase α, and, in order to account for these effects, we must extend the single-component multiphase flow theory to one involving many components. This extension is discussed in the following section.

7.2.5. Multiphase–multicomponent flows

While it is possible to assign unique properties to each chemical constituent or component in a mixture (Bowen, 1976), we will not follow this approach in order to keep the model as simple as possible. In our approximation, we only modify the conservation of mass equation of each phase to account for the diffusion of each

constituent and retain the previously-derived phasic conservation equations for momentum, energy, inertia, and dilatation–contraction transport.

If $\omega_{a\alpha}$ is the mass fraction of constituent a in phase α, Equations (7.24) and (7.25) need to be replaced by

$$\frac{\partial \bar{\rho}_\alpha \omega_{a\alpha}}{\partial t} + \frac{\partial \bar{\rho}_\alpha \omega_{a\alpha} v_{\alpha j}}{\partial x_j} = \hat{c}_{a\alpha} - \frac{\partial J_{a\alpha j}}{\partial x_j}; \quad a = 1, \ldots, s \tag{7.35}$$

$$\frac{\partial \bar{\bar{\rho}}_\alpha \omega_{a\alpha}}{\partial t} + \frac{\partial \bar{\bar{\rho}}_\alpha \omega_{a\alpha} v_{\alpha j}}{\partial x_j} = \frac{\hat{c}_{a\alpha}}{\phi_\alpha} - \bar{\bar{\rho}}_\alpha \varphi_\alpha - \frac{1}{\phi_\alpha} \frac{\partial J_{a\alpha j}}{\partial x_j}; \quad a = 1, \ldots, s \tag{7.36}$$

where $\hat{c}_{a\alpha}$ is the net mass generation rate per unit volume and $\mathbf{J}_{a\alpha}$ is the *mass diffusion flux* of constituent a in phase α. $\hat{c}_{a\alpha}$ accounts for the combined effects of nucleation, condensation, evaporation, aggregation, fragmentation, and chemical reactions. The constituent mass generation rate is equal to zero if no constituent is produced or consumed, while its mass flux can be produced with or without chemical reactions. Conservation of mass of each chemical constituent then requires

$$\sum_{a=1}^{s} \omega_{a\alpha} = 1, \quad \alpha = 1, \ldots, \gamma; \quad \sum_{a=1}^{s} \hat{c}_{a\alpha} = \hat{c}_\alpha, \quad \sum_{\alpha=1}^{\gamma} \hat{c}_\alpha = 0 \tag{7.37}$$

The diffusion flux $\mathbf{J}_{a\alpha}$ accounts for the diffusion of component a relative to the mean flow of phase α and, according to the kinetic theory (Hirschfelder et al., 1954), it is proportional to the mass fraction gradient

$$\mathbf{J}_{a\alpha} = -\mathbf{K}_{a\alpha} \cdot \nabla \omega_{a\alpha} \tag{7.38}$$

where $\mathbf{K}_{a\alpha}$ is the *mass diffusion tensor* that accounts for the effects of turbulence.

The Eulerian formalism is useful for modeling the continuous gas phase and large number of fine particulate phases of the mixture because these strongly interact with each other through collisions and turbulence. The large particles, on the other hand, are affected much less by the gas and small particulate motions and tend to follow ballistic trajectories. Their motions are more easily described by kinetic equations.

7.2.6. Coarse–particle kinetic equations

Large particles can collide and fragment into smaller particles in a volcanic plume. Particles can aggregate into larger particles when they are wet, because of the condensation of plume volatiles and scavenging action of fine particulates. Large particles fall to the ground in the form of raindrops, pumices, accretionary lapilli, and blocks. Aggregation is particularly effective in phreatomagmatic eruptions because of the large releases of water vapor into the atmosphere. The deposits of Phlegraean Fields and Vesuvius supply ample evidence of the fallout of such particulate matter during the eruptions of these volcanoes (Cioni et al., 1992; Rosi, 1992). As discussed above, coarse particles can be grouped into clusters according to Equation (7.5), with m_c being the particle cluster mass, $\mathbf{v}_c$ the particle cluster velocity, and h_c the particle cluster enthalpy. Each cluster c consists of N_c particles

and this number changes temporarily and spatially. The conservation of mass, momentum, and energy for each cluster can then be written as follows:

Conservation of mass:

$$\frac{dm_c}{dt} = \hat{\omega}_c, \quad c = 1, \ldots, n \tag{7.39}$$

where $\hat{\omega}_c$ is the mass generation rate for cluster c, and it includes mass change from volatilization, evaporation and condensation, chemical reactions, fragmentation, and aggregation.

Conservation of momentum:

$$\frac{dm_c \mathbf{v}_c}{dt} = \mathbf{F}_c + m_c \mathbf{g} + \hat{\omega}_c \mathbf{v}_c \tag{7.40}$$

In this equation, $\mathbf{F}_c$ is the resultant surface force and $\mathbf{g}$ the resultant body force per unit mass acting on the particles of cluster c. The resultant force is produced from the stress τ_c acting on the particles of c

$$\mathbf{F}_c = \int_{A_c} \tau_c \cdot \mathbf{n}\, dA \tag{7.41}$$

where A_c is the surface area of particles belonging to c and $\mathbf{n}$ is the unit normal vector to A.

Conservation of angular momentum:

$$\frac{d(\mathbf{I}_c \cdot \boldsymbol{\omega}_c)}{dt} = \int_{A_c} \mathbf{r}_c \times (\tau_c \cdot \mathbf{n}) dA + \mathbf{N}_c \tag{7.42}$$

where $\mathbf{I}_c$ is the inertia tensor and $\boldsymbol{\omega}_c$ the angular velocity of cluster c. $\mathbf{r}_c$ is the position vector from the center of rotation to the center of mass of the cluster, and $\mathbf{N}_c$ is the resultant moment acting on c.

Conservation of energy:

$$\frac{dm_c H_c}{dt} = \dot{Q}_c + m_c r_c + \hat{\omega}_c H_c + \mathbf{F}_{ct} \cdot \mathbf{v}_c \tag{7.43}$$

where H_c is the total enthalpy which consists of cluster (specific) enthalpy h_c, cluster kinetic energy $\frac{1}{2} v_c^2$, and cluster potential energy gz, where z is the height above the surface of the volcano. $\dot{Q}_c$ is the rate of heat transfer to the cluster, r_c is the cluster heat generation rate, and $\mathbf{F}_{ct}$ is the resultant tangential force acting on cluster particles.

Equations (7.39)–(7.43) must be solved together with the equations of Sections 7.2.4 and 7.2.5 and an appropriate set of constitutive equations which account for specific materials exchanging mass, momentum, and energy in the mixture.

7.2.7. Additional modeling considerations

The material transport model described above is sufficiently general to be able to model a wide variety of processes in volcanic eruption columns. These include

particle–particle and particle–gas interactions, phase changes, and chemical reactions between the constituents of the mixture.

The mass transport Equations (7.35)–(7.39) include phase changes and chemical reactions, the momentum Equations (7.26) and (7.40) allow for the exchange of forces between the constituents of multiphase mixture, and the energy transport Equations (7.28) and (7.43) allow for the exchange of heat and work between the phases and chemical constituents of the mixture. The inertia and dilatancy transport Equations (7.30) and (7.31) include the effects of averaging over small scales of the flow and thus provide a feedback between the small and large scales of the flow. The coarse-particle angular momentum Equation (7.42) accounts for the effects of spins of large particles. The distribution of different size particles in the plume as given by Equation (7.4) is more restrictive than the mass conservation Equations (7.35) and (7.36), because the mass generation rate $\hat{c}_{a\alpha}$ in these expressions can include more general constitutive relations than those on the right side of Equation (7.4).

The Eulerian transport equations can be written in the following general form

$$\frac{\partial \Phi_\alpha}{\partial t} + \nabla \cdot \mathbf{v}_\alpha \Phi_\alpha + \nabla \cdot \mathbf{J}_\alpha = S_\alpha, \quad \alpha = 1, \ldots, m+1 \tag{7.44}$$

where Φ_α is a vector of dependent variables, $\mathbf{J}_\alpha$ are the fluxes, and S_α are the source terms of Eulerian phases. The coarse-particle kinetic equations can be expressed as follows

$$\frac{d\Phi_c}{dt} = S_c, \quad c = 1, \ldots, n \tag{7.45}$$

where Φ_c and S_c are the coarse-particle dependent variables and sources, respectively. The conservation law form of Equation (7.44) is suitable for numerical solution as further discussed in Section 7.3.

In order to investigate the mathematical structure of Equation (7.44), it is convenient to rewrite it in the form of primitive variables

$$\frac{\partial \Phi_\alpha}{\partial t} + \mathbf{A} \cdot \nabla \Phi_\alpha = \tilde{S}_\alpha \tag{7.46}$$

where the matrix $\mathbf{A}$ and source terms $\tilde{S}_\alpha$ do not contain any derivatives of dependent variables. The system given by Equation (7.44) is hyperbolic whenever all eigenvalues of the matrix $\mathbf{A}$ are real and distinct, and this implies that the eigenvectors corresponding to the eigenvalues of $\mathbf{A}$ are linearly independent. When some of the eigenvalues are complex, however, the problem becomes ill-posed and renders any numerical finite difference method prone to numerical instability. This may occur, for example, when some void fractions become equal to zero. Dobran et al. (1993) avoided this difficulty by switching to single-phase flow calculations whenever the void fractions fell below 10^{-15}.

7.3. NUMERICS

As indicated in previous sections, volcanic eruptions are characterized by a wide spectrum of both time and length scales. This together with the length scales that are to be solved in order that a Global Volcanic Simulator be a faithful prediction tool require that a great deal of attention be paid to the discretization of the governing equations. Previous numerical techniques used in the studies of volcanic plumes have, in most cases, dealt with two-dimensional flows and conventional upwind discretizations of the advection terms in the momentum and energy equations (Valentine and Wohletz, 1989; Dobran et al., 1993, and subsequent works using the same computer code). Higher-order upwinding schemes use flux-limiters techniques (Sweby, 1984; Leonard and Mokhtari, 1990) in order to avoid numerical instabilities. Some of these techniques also use an immersed boundary method to describe the volcano topography. This technique is based on the introduction of source terms into the continuity, linear momentum, and energy equations that mimic the presence of an immersed, no-slip boundary (Kim et al., 2001).

While first-order accurate upwind discretizations enhance the diagonal dominance of the coefficient matrices and avoid unphysical oscillations at mesh Reynolds numbers larger than 2, they produce a large amount of artificial viscosity that, in addition to being larger than the physical one, produces smearing. This effect is particularly important in the case of volcanic eruptions where shock waves may be present and the typical dimensions may be on the order of 50 km in height and 100 km in diameter. If, for such conditions and in the absence of crosswind, we assume a kinematic viscosity identical to that of the air at standard pressure and temperature, that is $\nu = 1.5\,\mathrm{m^2\,s^{-1}}$, and a characteristic velocity on the order of $50\,\mathrm{m\,s^{-1}}$, and a $100 \times 100 \times 100$ grid, so that the mesh size is on the order of 1 km, the mesh Reynolds number is much larger than 2 and an upwind discretization of the advection terms introduces an artificial (kinematic) viscosity on the order of $10^4\,\mathrm{m^2\,s^{-1}}$. This viscosity is much larger than the kinematic viscosity of air and produces a much more viscous flow than the one that we are trying to resolve. A similar comment applies to meteorological predictions based on first-order upwind discretizations of the advection terms in coarse grids. Note that our estimates are based on laminar flows and that these are overestimates, since volcanic eruptions involve turbulence which produces turbulent viscosities that are usually much larger than laminar ones, except near the ground.

Although the amount of artificial viscosity can be somewhat reduced by higher-order upwind discretizations of the advection terms, the resulting finite difference equations are less stable and robust, require more grid points, and, therefore, pose more difficulties in the imposition of boundary conditions than first-order upwind differences (Morton, 1966). In spite of being claimed that the use of locally one-dimensional methods based on the solution of linear advection–diffusion equations can yield less artificial diffusion than first-order upwind techniques, these claims are incorrect, for it can be easily shown that, at large mesh Reynolds numbers, these techniques become first-order accurate upwind methods.

In addition to the issue raised above, attention should also be paid to the 'irregularity' of the topography of the surroundings of a volcano as well as to the effects of crosswinds that deflect the pyroclastic plume (Oberhuber et al., 1998; Graf et al., 1999) and affect both its dynamics and thermodynamics in a different manner in the windward side than in the leeward one. The fact that the topography is irregular not only affects the flow near the ground, but also the discretization of the governing equations in a major manner and opens an interesting issue related to the employment of structured or unstructured grids (Ollivier-Gooch and Van Altena, 2002). Although unstructured grids are more versatile and can be adapted to irregular boundaries more easily than structured ones, they have the inconvenience that one must keep track of the vertices and sides of control volumes to either make the appropriate interpolations or approximate the fluxes at interfaces when either finite difference or finite volume methods are employed for the discretization of governing equations of Section 7.2.

An alternative to unstructured grids is the use of local grid generation techniques that map an irregular part of the flow domain into a regular one and thus allow for the concentration of grid points in the regions of high-flow gradients or boundary curvature. Although the smoothness of these grid generation methods can, to a large extent, be controlled by means of elliptic grid generator methods, one should note, for example, that, sufficiently high above the ground, standard structured grids are more convenient. The grid lines at the interfaces between these grids and those obtained by local grid generation may, however, not coincide or, if they do coincide, may exhibit cusp points. In addition to the above issues, attention should also be paid to the conservation characteristics of the discretization of governing equations, especially when shock waves are produced near the volcanic vent.

This section consists of several parts. In Section 7.3.1, a DD method at the physical level is presented. Then, in Section 7.3.2, the discretization of the governing Eulerian equations by means of a finite volume formulation in each domain is discussed and a brief description of the system of (discretized) algebraic equations is presented. Section 7.3.3 deals with the discretization of Lagrangian equations. A special attention to the verification of the accuracy of the numerical plume dispersion model is presented in Section 7.3.4. A description of the parallel computer implementation of the finite volume method in unstructured meshes is presented in Section 7.4.

7.3.1. Domain decomposition at the physical level

As indicated above, the spatio-temporal dynamics and thermodynamics of volcanic eruptions involve a large spectrum of length and time scales; that is, shock wave formation and propagation, air entrainment, coagulation, tephra fallout, etc., several phases, and an irregular 'topography'. In addition, the presence of crosswind affects the plume dynamics and thermodynamics.

Due to the large number of scales that characterize volcanic eruptions, the physical domain has been partitioned into several overlapping subdomains as indicated in Fig. 7.3. The domains can be classified into two main categories: Regular

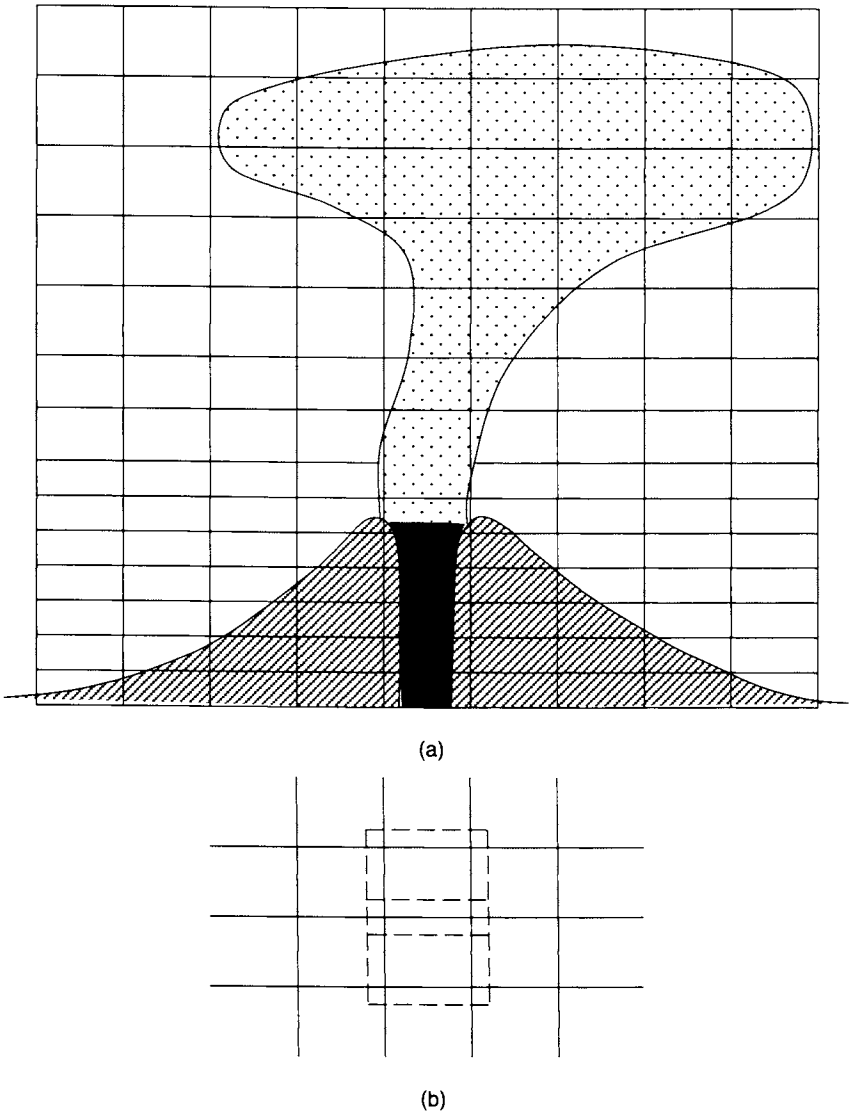

Fig. 7.3. Schematic illustration of a mesh around a volcano including the plume (a) and detail of overlapping subdomains/blocks (b).

and irregular domains. Irregular domains are those that are located near the ground and are adapted to the topography of the volcano surroundings. Roughly speaking, these domains can be defined as those between an imaginary plane perpendicular to the axis of and above the volcanic vent and the ground, and may be characterized by large aspect ratios. The regular domains, on the other hand, extend from this imaginary plane to the maximum height which is used as a boundary. This height may be located in the strastosphere or above, depending on the intensity of the eruption.

When crosswinds are present, the plume is deflected and the computational domain has to be extended in the leeward direction in order to follow this deflection. This may be accomplished by adding irregular and regular domains in such a manner that the plume is always located within the computational domain. In addition, some of the domains in the windward side can be eliminated. The addition and deletion of domains is performed in such a manner that the conservation of mass, momentum, and energy are ensured by using interpolation and global conservation principles. This has the advantage that the whole computational domain is being adapted to the crosswind and lateral motion of the plume in a quasi-static fashion. This quasi-static domain adaption technique is somewhat analogous to mesh refinement techniques where grid points are added/deleted as the solution evolves, such as, for example, in the *h*-version of the finite element method (Demkowicz et al., 1985). Such an adaption is based on the lateral deflection of the plume from the crosswind velocity, time step used in the simulations, and a safety factor in order to ascertain that the plume is always located within the computational domain. Since the grid is enlarged in the leeward side of the plume and may be decreased in the windward one, and, since the wind direction may vary with time, this adaption technique is a general one and may result in a large number of domains in the direction of the wind and a small number of domains in the transversal direction.

As indicated above, the addition and deletion of subdomains has to be performed in such a manner that the global conservation properties are not violated. This can be achieved by imposing the appropriate fluxes on the faces of the domains that are added and by modifying those near the ones removed. This does not pose any problems if the domains added in the leeward side or deleted in the windward side are sufficiently far from the plume.

The reason for using overlapping rather than non-overlapping domains is that at the interface of the latter the continuity and smoothness conditions of the flow variables have to be imposed, because the interface between two adjacent non-overlapping subdomains is a sharp one. Such conditions of continuity and smoothness do not necessarily ensure conservation of fluxes normal to these interfaces, and require the use of Dirichlet–Neumann, Dirichlet–Robin, or Neumann–Robin cycles in adjacent subdomains to achieve convergence in an iterative fashion. These iterative cycling techniques have been shown to converge for strictly elliptic problems in smooth domains, but their rate of convergence deteriorates drastically if the domains are non-smooth, that is if one of the domains exhibits sharp corners (Ramos and Soler, 2001).

7.3.1.1. Multiblock strategy

The basic idea of this strategy is to break up the domain into several smaller blocks (essentially an ultra coarse mesh) and then generate separate meshes in each individual block (Eriksson, 1982; Eiseman, 1985). Fig. 7.4 illustrates this idea by showing a schematic of a block decomposition for the region near the ground. This figure shows that a subdomain is geometrically much simpler than the full

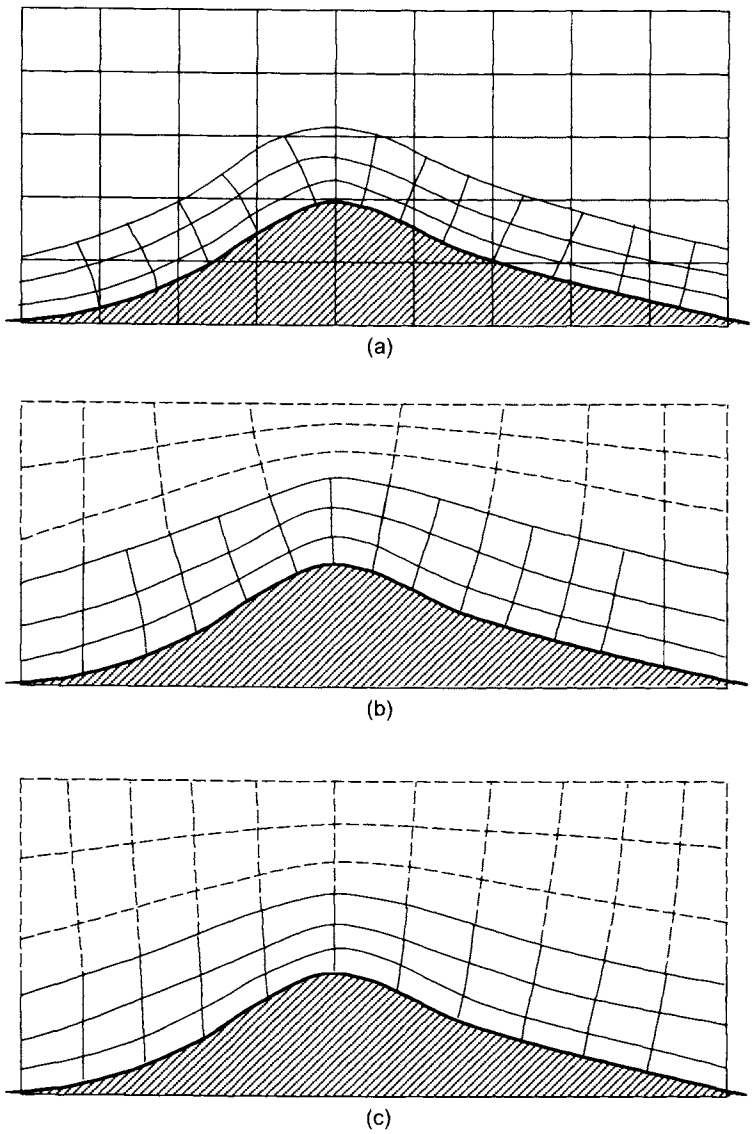

Fig. 7.4. Overset mesh combination (a), patched mesh combination (b), and composite mesh combination (c).

configuration and that, therefore, it can be easily meshed either by solving a partial differential equation or, alternatively, by using an algebraic method. It is, in fact, common practice nowadays to create the mesh in any particular block by an algebraic method such as transfinite interpolation and then smooth the mesh by some iterations of an elliptic solver (Eriksson, 1982; Eiseman, 1985).

There are several variants of the multiblock technique, depending on whether or not continuity of mesh lines is maintained across the block boundaries. Overset

methods (Fig. 7.4a) represent one extreme situation where no attempt is made to match meshes from neighboring blocks or subdomains (Chesshire and Henshaw, 1990). The lack of any constraint at the subdomain boundaries means that mesh generation for the individual subdomains is much easier. In particular, there is no *a priori* need to create block interfaces and this advantage has facilitated an early application of the overset approach to complicated geometries. Another advantage of permitting such a loose connection between neighboring meshes is the possibility of treating moving body problems. Since the penalty for these advantages lies in the need to transfer information between neighboring meshes, this requires a means of determining an appropriate overlap region and the development of interpolation formulae to ensure accurate data transfer.

A patched multiblock mesh (Fig. 7.4b) has an *a priori* defined block structure with blocks that conform with their respective block boundaries, but without the need to maintain continuity of mesh lines between neighboring blocks. Interpolation at block boundaries is now less demanding than that required by an overset system. This approach has the advantage of allowing a highly refined mesh in specific regions without imposing unnecessary refinement elsewhere. A composite multiblock mesh (Fig. 7.4c) can be regarded as a special case of the patched approach in which the mesh lines are required to be continuous across block interfaces, that is, subdomains (Thompson, 1987). This has the drawback that the mesh refinement in one block, involving an increase in the number of mesh points on block boundaries, will induce a corresponding refinement in neighboring blocks and so on throughout the mesh. It does, however, ensure continuity of the mesh lines. Mesh smoothness is further enhanced by requiring slope continuity across block interfaces as well. Although a composite multiblock mesh is more difficult to create than an ordinary patched multiblock one, it has significant advantages (usually there is no need to interpolate the solution) that arise from the continuity of mesh lines. It is, therefore, not surprising that most of the commercial computational fluid dynamics (CFD) codes now offer structured mesh generators that exploit a composite multiblock approach (Thacker, 1980).

The requirement to define the position and mesh discretization of the block interfaces remains a largely manual task. A good graphics user interface (GUI) can ease the burden of creating the block structure, but it can still be a time-consuming process. More significantly, the difficulty of automating this process inhibits the use of composite block methods for solving time evolving problems, or other situations such as automatic design, where the boundary shape is changing. It may then be necessary to alter the block interface positions, or even the block arrangement and connectivity (block topology), leading to potentially insurmountable difficulties if automated blocking is not possible.

Multiblock and structured mesh generation techniques have improved steadily over the last 20 years and have reached a state of relative maturity. Commercial software is now available that provides the user with a GUI to create multiblock meshes around configurations of essentially arbitrary complexity. In practice, new meshes are often required for configurations whose overall shape is not too different from the one analyzed in a previous computer run. Aerodynamic design, for

example, may require many runs to develop a new wing or to determine the optimum placement of a nacelle. Slight changes in wing shape or nacelle alignment do not affect the block topology which remains unchanged from one run to the next. It is, therefore, not surprising that topology libraries containing templates for the block decomposition of different aircraft configurations are now used extensively throughout the aircraft industry to ease the difficulties associated with the construction of a multiblock mesh.

The user is still forced to identify and construct the required bounding interfaces for each multiblock subdomain whenever a radically new configuration is considered, and thus the lack of an automated blocking capability remains a major weakness of all multiblock methods. Despite the development of several user-friendly utilities to assist in this task, generating new multiblock decompositions for structured meshes remains a time-consuming task involving an excessive amount of human interaction.

7.3.1.2. Cartesian methods

It is generally accepted in CFD that a boundary conforming mesh is desirable to achieve accurate solutions from any numerical solver. If one is willing to sacrifice this requirement, the mesh generation becomes a much simpler task. Difficulties arise at the boundary where the Cartesian mesh intersects the boundary surface. Although finite difference methods can be derived to interpolate the boundary conditions onto the nearest mesh points, it is difficult to ensure solution accuracy. If extra points are inserted where mesh lines intersect the surface, however, it is then possible to create a boundary conforming mesh. In this respect, boundary conforming Cartesian methods are seen to be closely related to Octree-based triangulation methods (Shephard and Georges, 1991; George and Borouchaki, 1998; Frey and George, 1999). In fact, the elements obtained from the Octree and their intersection with the boundaries are precisely the elements that make up the Cartesian mesh (Fig. 7.5). Conversely, any Cartesian mesh can be converted into an Octree type triangulation by splitting all elements into tetrahedra (triangles in two dimensions).

Most of the elements in a Cartesian mesh will be hexahedra, although the elements adjacent to the surface can be expected to assume a variety of polyhedral shapes, depending on the way in which an Octree hexahedron intersects any given region of the boundary surface. A Cartesian mesh is, therefore, well suited for use by a finite volume or finite element method that can accept arbitrarily shaped elements. Given the close affinity between Cartesian meshes and Octree-based triangulations, it is to be expected that they share the same advantages and limitations. In particular, the problems of correctly finding the intersection between the Cartesian/Octree mesh and the boundary surface, identifying the element shapes for the intersected Cartesian cells, and adequately refining the mesh near small boundary features are substantial. Cartesian mesh methods also suffer from the drawback that the surface discretization is not known beforehand and it is, therefore, often difficult to ensure a good surface mesh quality. On the positive side, the surface

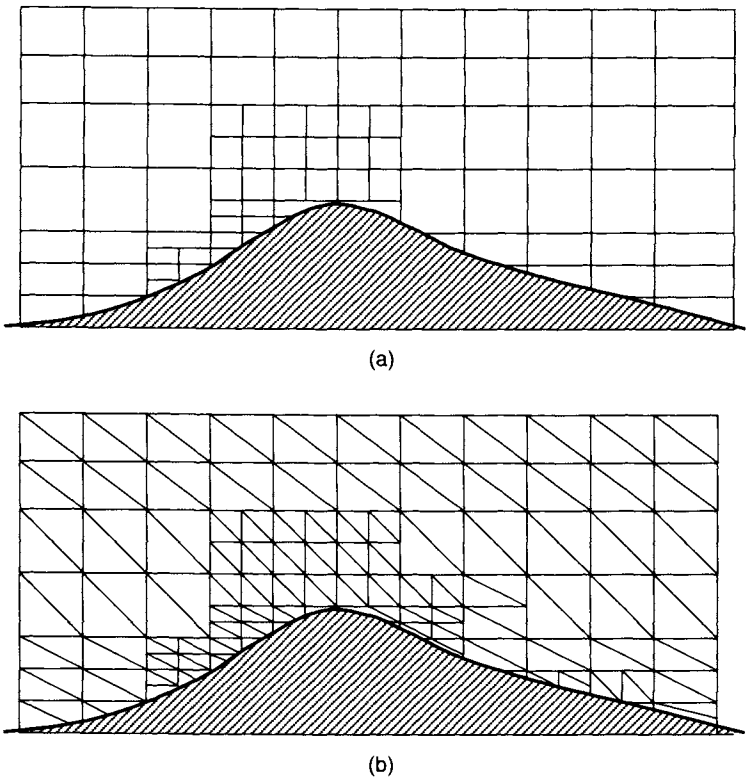

Fig. 7.5. An Octree decomposition near the ground (a) and conversion of the Octree decomposition into a triangulation (b).

discretization is a by-product of volume discretization and it is, therefore, possible to generate meshes around highly complex geometries without the need for carefully crafted surface meshes. In fact, the surface definition can be obtained directly from the CAD description, provided there is a utility to determine the intersection of a given line with the surface. Since Cartesian and Octree-based mesh generation methods circumvent the need for prior creation of a surface mesh, a significant advantage is achieved in the turnaround time from the design prototype to the flow solution.

7.3.1.3. Mesh near the ground

As stated above, volcanic eruption plumes are turbulent and turbulence is one of the unsolved problems of physics which is characterized by a very broad spectrum of time and length scales. This disparity in length scales produces a difficulty for appropriately resolving turbulence except for flows in simple geometries at low Reynolds numbers. This implies that turbulence modeling of volcanic plumes is necessary (Section 7.2) in order to account for small scales, and that this modeling will have a major impact on mesh generation, especially near the ground where

there is a need to create highly stretched mesh elements inside boundary and shear layer regions.

There is a reasonable body of experience with structured meshes that justifies their use for Navier–Stokes computations. For unstructured meshes, there is less evidence to draw on and there is a general suspicion that highly stretched tetrahedra are not suitable mesh elements for the computation of viscous layers in high Reynolds number flows.

The generation of anisotropic, or highly stretched, elements poses a number of difficulties in the mesh generation process. In particular, it is necessary to maintain careful control over point placement and mesh connectivity to ensure adequate mesh quality; that is, the element interior angles should not be much larger than 90 degrees, high aspect ratio elements should be aligned with the boundary surface, etc. These problems have been addressed in various ways by means of:

1. Tetrahedral mesh-mapping techniques that apply an affine transformation to a triangulation so as to create an anisotropic layer of elements (Mavriplis, 1990, 1995; Peraire et al., 1992).
2. Tetrahedral mesh-advancing layers methods that introduce an advancing layers method to create anisotropic meshes wherever boundary layers can be expected by, for example, extruding tetrahedra (Pirzadeh, 1996).
3. Hybrid meshes (Kallinderis et al., 1996).

It is known that the truncation error of a finite volume discretization depends on the shape of the control volume. In particular, a trapezoidal approximation for a vertex-based method, though nominally second order, becomes first-order accurate unless the control volume possesses central symmetry. For a vertex-based discretization, the control volume associated with a given point typically corresponds to the boundary of the collection of elements incident at that point. For a cell-centered discretization, it is the element boundary that functions as the control volume. On a structured mesh of hexahedra, one can generally expect central symmetry at all mesh points unless there are extreme distortions in the mesh. A planar triangulation will have central symmetry if the triangles are all equilateral, resulting in hexagonal control volumes for vertex-based schemes. In an anisotropic layer of highly stretched triangles, the central symmetry can only be achieved if the mesh maintains a structured appearance (that is, advancing layers) and all the diagonal edges are oriented in the same direction. In a tetrahedral mesh, however, it appears impossible to achieve the central symmetry under any circumstances. If this is the case, it is then necessary to maintain this symmetry of control volumes in boundary layer regions.

If prism-shaped elements are used in the viscous layer, the central symmetry will be preserved, provided that there is good triangle quality in the lateral direction parallel to the boundary surface. By combining prismatic elements with a tetrahedral mesh, one might expect to achieve solutions of Navier–Stokes equations that match the accuracy of computations on structured hexahedral meshes. Since the prism layer is unstructured in the lateral direction, there is much more flexibility in handling complex geometries and a greater opportunity to achieve a high level of automation in the mesh generation process than would be the case with purely

hexahedral elements. For these reasons, hybrid meshes of prisms and tetrahedra have considerable appeal as the best compromise to achieve accuracy in turbulent computations while permitting ease of mesh generation for complex configurations.

It must be pointed out, however, that there is little hard evidence to support the contention that using prisms in the boundary layer region is more accurate than using tetrahedra, or that hybrid meshes achieve the same accuracy as composite multiblock meshes made up of hexahedra. Structured multiblock methods achieve good accuracy, but are time consuming to apply. Tetrahedral meshes with anisotropic elements in boundary layer regions are easier to create, but their accuracy is suspect. Overset methods represent a compromise between ease of use and their purported solution accuracy for viscous flows.

It seems likely that the trade-off between accuracy and ease of use will shift, so that, perhaps, one of the meshing methods will stand out as clearly superior in meeting the dual requirements of solution accuracy and ease of application. In the best of all possible worlds, one might hope that all mesh generation methods would one day meet this goal. At the time of writing, it appears that composite multiblock meshes of hexahedra offer the best accuracy for turbulence computations, but the lack of an algorithm for automated block decomposition renders these meshes time consuming to create. At the other extreme, the Cartesian approach offers essentially fully automated mesh generation, but the poor quality of mesh elements near boundary surfaces severely limits the accuracy of these mesh types, particularly for turbulent computations. Overset meshes of hexahedra represent a compromise that lies between these two extremes; they are more complicated to set up than tetrahedral meshes and computations on overset meshes are arguably less accurate than comparable computations on composite multiblock hexahedral meshes. In fact, our recent experience suggests that the accuracy achieved on carefully constructed overset meshes may be on a par with the accuracy obtained by computations using composite multiblock meshes.

Accurate and fast simulations of volcanic eruptions depend on the rapid turnaround of many computer simulations involving several million mesh points. This requirement places a premium on computational efficiency and can often influence the choice of mesh type. Most vertex-based methods, for example, exploit an edge-based data structure so that the computational efficiency is directly related to the number of edges in a mesh. For a given number N of mesh points, the number of edges in a hexahedral mesh is approximately $3N$, the number of edges in a mesh made entirely of prisms is approximately $4N$, while a tetrahedral mesh contains roughly $7N$ edges. All other things being equal, prisms should be preferred over tetrahedra when running edge-based flow solvers. Likewise, hexahedra should be preferred over both prisms and tetrahedra. The construction of hybrid meshes, containing large regions meshed by hexahedra wherever this can be easily accomplished, is a common practice for both laminar and turbulent flow computations.

Whether automated blocking is possible for composite multiblock meshing has been an open question for the last 20 years and it is likely to remain so without radical new insights. In the absence of a satisfactory answer, it seems reasonable to

look for ways that might lead to some degree of automation and thereby reduce the amount of human labor that is needed to create composite multiblock meshes around highly complicated configurations. One option might lie in exploiting the high degree of automation achieved by tetrahedral meshing methods. It is possible that this geometric structure could be used to guide the decomposition of the flowfield into large hexahedral blocks, leading to a partial resolution of the automated blocking problem.

Alternatively, one may ask whether the accuracy of flow computations run on tetrahedral meshes could be improved to match the accuracy attained on comparable composite multiblock hexahedral meshes. To achieve this goal, it will be necessary to reach a deeper understanding of the relation between element type and the accuracy of the discretization formulae that are used to approximate the flow equations, particularly on highly stretched meshes. This depends, of course, on the way in which the flow equations are discretized, since different flow solvers can be expected to exhibit varying degrees of sensitivity to different mesh types. As an example of the subtle interplay between mesh stretching and the flow solver algorithms, one notes how the least-squares approach for estimating flow gradients can be quite inaccurate in boundary layer regions. This often results in increased artificial dissipation in the boundary layer, leading to a less accurate flow solution and poorer estimates of flow friction. Much more work needs to be done to understand how mesh behavior influences the accuracy of discretization formulae and to what extent one can build flow solvers that are reasonably tolerant of mesh imperfections and idiosyncracies.

The success of tetrahedral mesh generation in achieving a high degree of automation has also moved attention to the more time-consuming aspects of mesh generation, namely surface mesh generation and the CAD interface. From the point of view of the user, an ideal black-box mesh generation system would consist of a seamless suite of software to clean up imperfections in the CAD description, automatically generate a surface mesh to meet a required mesh density, and then create a volume mesh. All this would, of course, be done at the push of two or three buttons to specify certain parameters, that is the accuracy to which the true surface is approximated, the height of the first element off the surface, the total number of mesh points, etc. As noted above, the Cartesian/Octree methods circumvent the need for surface mesh generation and can, in principle, be linked directly to a CAD interface.

Is it perhaps not too far fetched to imagine that different mesh generation methods might one day combine to achieve the goal of black-box mesh generation. For example, a Cartesian volume meshing method might be used to obtain an initial surface triangulation that could be adaptively improved to produce a good quality surface triangulation. A tetrahedral mesh generator could take this surface triangulation and reliably create a good quality volume mesh of tetrahedra. If, as suggested above, this tetrahedral mesh could be exploited to achieve a semi-automated block decomposition of the flow field, then a composite multiblock hexahedral mesh could be generated with little need for human intervention.

7.3.2. *Finite volume discretization of the Eulerian equations*

In each block/subdomain, the Eulerian equations presented in Section 7.2 are discretized by means of finite volumes in space. Both collocated and staggered grid arrangements can be used (Fig. 7.6). Due to the disparate time and length scales involved in volcanic eruption plumes, the governing equations are stiff. Therefore, if explicit methods were used to solve the discretized form of the governing equations, the time step would be controlled by the fastest decaying process and a large number of time steps would be required to perform a volcanic eruption simulation. This can be avoided by using an implicit discretization which requires an iterative procedure for the solution of the discretized equations in each subdomain and may

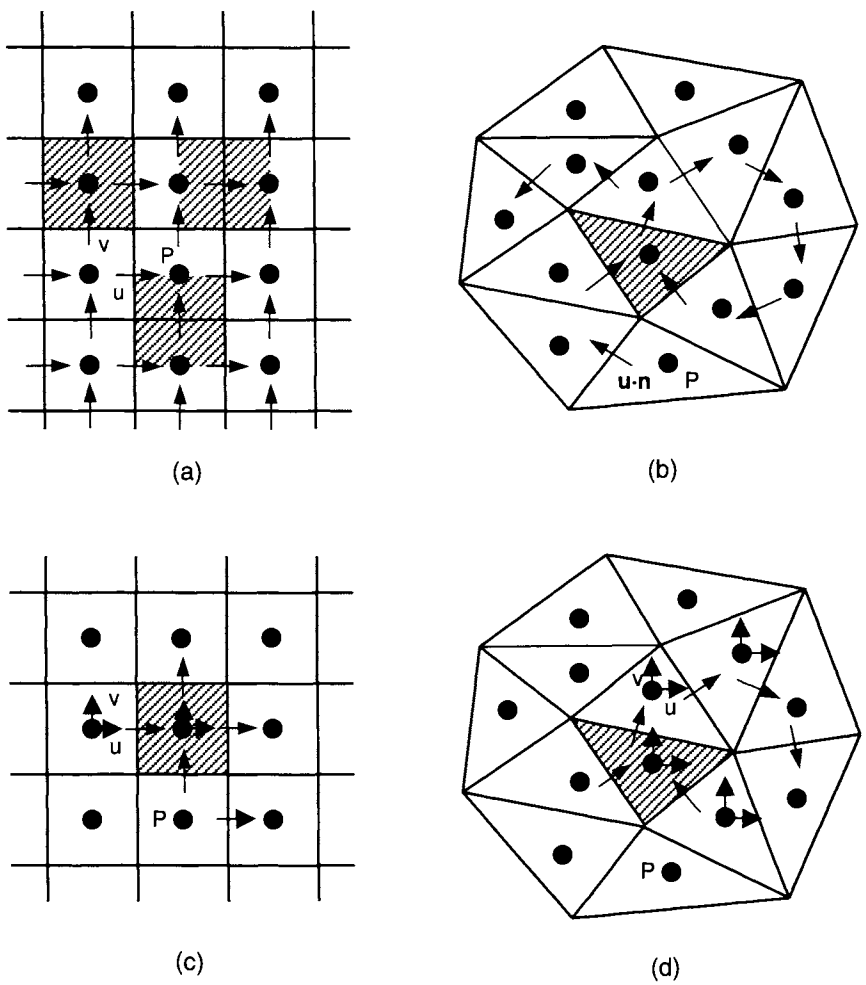

Fig. 7.6. Schematic of the staggered (a) and (b) and collocated (c) and (d) schemes for structured (a) and (c) and unstructured (b) and (d) meshes.

pose some communication problems amongst the different processors when parallelism is used to solve these equations.

The discretization of Eulerian equations is based on cell-centered grids, first- or second-order accurate time-linearization with respect to the previous time level, and second-order accurate spatial discretizations for the source and diffusion-like terms. The time-linearization results in linear partial differential equations in space at each time level.

The advective fluxes are discretized by means of a weighted essentially non-oscillatory (WENO) method (Jiang and Shu, 1996; Shu, 1996) that is second-order accurate in non-smooth regions and third-order accurate in smooth ones. This method is based on a Lagrange interpolation of the cell-centered quantities to determine the advective fluxes and includes smoothness indicators. These indicators measure the smoothness of a particular interpolation polynomial and are related to the L^2-norm of all the derivatives of the interpolation polynomial. Some advantages of this technique include its third-order accuracy in smooth regions, second-order accuracy in non-smooth regions such as shock waves, use on unequally spaced grids, and the elimination of the loss of accuracy associated with total-variation diminishing (TVD) and essentially non-oscillatory (ENO) techniques near discontinuities. In addition and due to the presence of smoothness indicators in WENO techniques, these methods can be easily employed for local grid adaptation. For example, one may evaluate the largest difference between different smoothness indicators in a single cell or control volume, and if this difference exceeds a user's specified value or the solution is not very smooth, the grid cells can be added by splitting the cell where this occurs into two new ones. In a similar fashion, one can merge two cells into one whenever the largest smoothness indicators drop below a user's specified lower threshold. The thresholds for cell splitting or merging are problem specific and have to be selected in a trial-and-error fashion. Moreover, in order to prevent loss of stability and accuracy when cell splitting is performed, the cell-centered values in the new grid should be determined in accord with WENO principles, that is, by integrating the interpolation polynomials over the new cells.

Using a time-linearization method for both Eulerian and Lagrangian (Section 7.3.3) phases, together with the discretization of spatial derivatives in each subdomain and the time-linearization of source terms, produces a linear system of algebraic equations of the form

$$\mathbf{A}\mathbf{x} = \mathbf{b} \tag{7.47}$$

where $\mathbf{A}$ is the coefficient matrix and $\mathbf{x}$ and $\mathbf{b}$ are the vectors of unknown and known quantities, respectively. The matrix $\mathbf{A}$ also includes the boundary conditions, which for the overlapping domains considered here are of the Dirichlet type and must be updated due to the coupling between adjacent subdomains.

As stated above, the spatial accuracy of the method considered here is second-order in non-smooth regions and third-order in smooth ones, whereas the time accuracy is either first- or second-order, depending on whether the time discretization is performed by means of a standard implicit or trapezoidal rule. First-order temporal accuracy may not be enough (because of large time steps that may have to

be used in order to predict the evolution of volcanic eruptions in a reasonable time) due to the accumulation of temporal discretization errors, and, especially, when the time step is much larger than the largest characteristic time of volcanic processes within the plume. In this case, the time-linearization technique which corresponds to a single iteration of the Newton–Raphson method can be replaced by a predictor–corrector method, where the predictor is the time-linearization method just described and the corrector is based on a quasilinearization method where the linearization is performed with respect to the previous iteration. Due to the quasilinearization, linear algebraic equations result at each iteration, and iterations have to be carried out as many times as required until a user's specified convergence criterion is satisfied. This iterative technique is of special interest, especially if approximate factorization methods are employed to reduce the computation of three-dimensional flow fields in a three-dimensional subdomain to a sequence of solutions of either one- or two-dimensional problems, due to the factorization errors introduced by the approximate factorization.

7.3.3. Discretization of the Lagrangian equations

As described in Section 7.2, the clusters of large particles will be treated in a Lagrangian fashion by accounting for their mass, linear and angular momenta, and energy exchanges among both themselves and those phases belonging to the Eulerian group. These mass, momentum, and energy equations are governed by nonlinear ordinary differential equations which are solved by a second-order time-linearization method, whereby the nonlinear terms are linearized with respect to the previous time level. This method results in linear algebraic equations at each time level and can be interpreted as the first iteration of an iterative Newton–Raphson technique. It has the inconvenience that the linearization is performed with respect to the previous time level, which may produce substantial errors (despite of its A-stability) if the time step is sufficiently large. This is not only due to the leading-order (temporal) truncation errors, but also because the clusters may cross several computational cells in a single time step where the flow characteristics are quite different from those where the linearization was performed. This disadvantage may, however, be reduced by using a predictor–corrector method whereby the predictor step is based on the time-linearization technique described above and the corrector step uses a weighted source term that depends on the time spent in different cells during the time step (Fig. 7.7). This means that, in addition to the three spatial coordinates that identify the location of a cluster and its mass, velocity, and energy, one must also account for the fraction of time that each cluster spends in a computational cell per time step as shown schematically in Fig. 7.7.

The time discretization of Lagrangian phases equations can be written as a system of linear algebraic equations

$$\mathbf{B}\mathbf{y} = \mathbf{c} \tag{7.48}$$

which can be either appended to the linear system for the Eulerian phases or treated separately from it. Appending the discretized Lagrangian equations to the

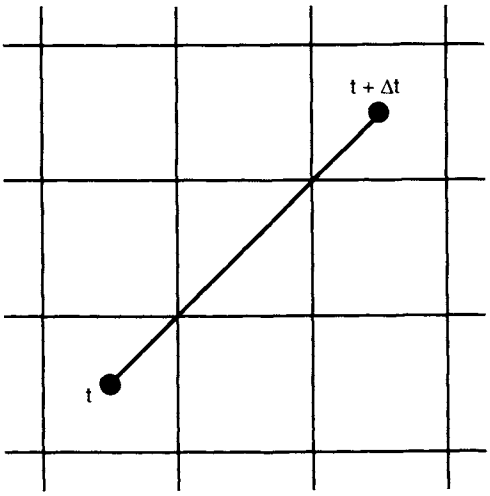

Fig. 7.7. Schematic illustration of the path of the Lagrangian cluster and the cells that it crosses in a time step. The fraction of time spent in each cell is used to determine the source terms of the Lagrangian phase.

discretized Eulerian ones in each subdomain is advisable, provided that the dimensions of the former are smaller than those of the latter and a large number of subdomains and grid points are used to solve the Eulerian phases. This is due to the fact that the Eulerian equations must be treated iteratively when overlapping DD is employed at either the physical level as described above or at the algebraic level as described below. On the other hand, if full time-linearization is employed for the Eulerian phases and grids on the order of $200 \times 200 \times 200$ grid points are used and DD at the physical level is not used, then the algebraic equations for the Lagrangian phases may be appended to those of the Eulerian phases, because the DD is only performed at the algebraic and hardware levels. Of course, a $200 \times 200 \times 200$ point mesh may be unsuitable to accurately predict the evolution of a volcanic plume, despite the fact that even coarser grids have been employed in previous multidimensional simulations of volcanic plumes and magma flow in volcanic conduits (Dobran et al., 1993; Ramos, 1999; Esposti Ongaro et al., 2002; Neri et al., 2003; Dartevelle, 2004).

7.3.4. Verification

CFD has advanced considerably in the last 20 years or so, and the approach adopted here represents an attempt to model volcanic plumes based on the modeling equations of Section 7.2. These equations and the numerical approach proposed above may undergo changes in the future, due to improvements in physical modeling, numerical algorithms, and computer hardware. In fact, as the computer hardware continues to improve and offer ever increasing amounts of memory and ever faster processors, it is inevitable that the application of improved CFD codes

to very large and complex problems such as volcanic eruptions will become a task of greater interest.

However, one should keep in mind that there are several reasons for the shortcomings of current CFD technology. This includes limitations of the discretization formulae, grid generation and coupling, and deficiencies in turbulence models. Perhaps the most important and overriding concern is the size of the mesh and the dependence of the flow solution on element type. It is, therefore, of paramount importance to assess the accuracy of the volcanic eruption simulator proposed here and attempt to provide quantitative answers to the question of how the accuracy of numerical flow simulations depends on mesh size and on element type. The analysis presented below offers a means of assessing these effects without having to make a detailed investigation into the discretization scheme or turbulence model. In other words, the approach is general enough to permit comparisons across a broad class of CFD methods, while being specific enough to provide useful insights.

Several recent papers have addressed the problem of code verification and the assessment of solution error (Oberkampf and Blottner, 1998; Rizzi and Vos, 1998; Roache, 1998b). It is generally acknowledged that the need for effective criteria to evaluate different CFD codes and quantify the accuracy of numerical computations is compelling, but finding suitable criteria remains an elusive goal.

Roache (Roache, 1994, 1998b) proposed using the Richardson extrapolation (Richardson, 1910) to study the effect of mesh refinement and introduced the concept of a Grid Convergence Index (GCI) based on this approach. He presents strong arguments in favor of applying this technique for the assessment of solution accuracy as well as code validation. Questions remain, however, on when and where Richardson extrapolation may be used.

As originally formulated and as discussed in texts on numerical analysis (Isaacson and Keller, 1966; Cheney and Kincaid, 2004), the Richardson extrapolation is presented as a technique to improve the accuracy of a finite difference approximation given a set of discrete equi-spaced function values, but it is not known whether or not this approach is valid for a finite volume mesh whose elements vary widely in size and shape. It is also not known whether or not this approach is also valid for different mesh types, such as tetrahedra and prisms as well as hexahedra, and whether or not it can be applied to meshes that are uniform refinements of an initial mesh, such as the one that one might obtain by adding a mesh point at the mid-point of all edges and splitting each volume element into eight new elements. In addition, it is not known whether or not the outcome of applying this technique depends on whether one considers the number of mesh elements or the number of mesh points. A framework for answering these questions in a setting that is general enough to draw conclusions that are independent of mesh type is as follows.

Suppose that a set of partial differential equations to be solved on a domain D, is represented by a discrete approximation on a mesh that corresponds to a partition of D containing N elements whose volumes are given by $V_j, j = 1, 2, 3, \ldots, N$. If f is a dependent variable, or some quantity derived from the dependent variables, one can write the pointwise error of the discrete approximation to f on the jth element as $E_j(\mathbf{x})$. The error $E_j(\mathbf{x})$ will, in general, be a function of the position vector

$\mathbf{x} = (x, y, z)$. The *global error* for the approximation to f can then be written as

$$E = \frac{1}{V} \sum_{j=1}^{N} V_j E_j(\mathbf{x}), \quad V = \sum_{j=1}^{N} V_j \tag{7.49}$$

If the mesh is sufficiently fine so that the local error can be written as

$$E_j(\mathbf{x}) = K_j(\mathbf{x}, h_j) h_j^p, \quad K_j(\mathbf{x}, h_j) = k_j + O(h_j) \tag{7.50}$$

with $h_j^3 \equiv V_j$, h_j being the local mesh size, and k_j being a constant, for all $\mathbf{x}$ within some neighborhood that contains the jth element. The *local error* is then

$$E_j \sim k_j h_j^p \tag{7.51}$$

throughout the jth element, and the global error can be approximated as

$$E \sim \frac{1}{V} \sum_{j=1}^{N} k_j h_j^{3+p} \tag{7.52}$$

If the original grid is refined so that the new mesh size is $h_j' = r h_j$, it can be easily shown that the global error in the new mesh is

$$E' \sim r^p E \tag{7.53}$$

If we now define the average mesh size as

$$h = \left(\frac{V}{N} \right)^{\frac{1}{3}} \tag{7.54}$$

then

$$\frac{E'}{E} \sim r^p = \left(\frac{h'}{h} \right)^p \tag{7.55}$$

from which it can be concluded that the global errors are

$$E' \sim C h'^p, \quad E \sim C h^p \tag{7.56}$$

where C is a constant.

Under these conditions, it is possible to apply Richardson extrapolation to eliminate the leading error term and obtain a more accurate estimate of the global quantity f. Alternatively, if the solution has been computed on three different meshes with three different sizes, one can use Richardson extrapolation to determine both the leading error term and the exponent p that represents the order of accuracy. The above argument shows that, by using meshes fine enough for the computation to be in the asymptotic range, this is a sufficient, but not a necessary condition for Richardson extrapolation to be applicable.

The above simple analysis allows one to investigate the dependence of solution error on mesh size and thus provides a useful tool for error assessment and code verification. However, one should try to equidistribute the global errors throughout the subdomains and to determine how the effective exponent p is affected by mesh

refinement. Error equidistribution can be dealt with by considering a fixed number N of subdomains and by minimizing the functional $G = E + \lambda V$ with respect to h_j, where λ is a Lagrange multiplier. For the conditions given above, this minimization yields

$$E_j = k_j h_j^p = -\frac{3\lambda V}{p+3} = E \tag{7.57}$$

The global error E is thus minimized if the pointwise error E_j is equi-distributed over the mesh. $E_j = E$ requires that the mesh size elements h_j associated with the jth element satisfy

$$h_j = \left(\frac{E}{k_j}\right)^{\frac{1}{p}} \tag{7.58}$$

Although not presented here, one can use a generalized Richardson extrapolation for determining the exponent p of error reduction, i.e. $E = F(h) + Ch^p + O(h^{p+1})$. This procedure involves a nonlinear equation to extract the error exponent p from computations of f on three different meshes. If the asymptotic range property does not hold, it is then possible that the generalized Richardson extrapolation will not admit a solution for the exponent p, or that the solution for p will be negative. In this case, one must conclude that either the meshes are insufficiently fine to be in the asymptotic range or that one or more of the computed approximations to f is defective, owing, perhaps, to a lack of convergence of the discretized computation.

7.4. COMPUTER IMPLEMENTATION

As discussed above, the time and space discretization of both the Eulerian and Lagrangian equations in each subdomain/block produce systems of linear algebraic equations at either each time level if time linearization is employed or at each iteration if the equations are solved in an iterative fashion. In either case, the use of overlapping domains/blocks does require the use of iterative techniques due to the coupling between adjacent domains. Moreover, the resulting system of linear algebraic equations may not produce a symmetric matrix, and this requires the use of a preconditioned Krylov subspace technique (Brown and Saad, 1990; Knoll and McHugh, 1995; Shadid, 1999) to obtain its solution. In addition, the length scales involved in volcanic plumes have a wide spectrum and, therefore, their accurate simulation demands the use of parallelism solution methodologies.

Although there have been many studies on the parallel implementation of the Krylov subspace technique and, especially, of the conjugate gradient method (Demmel et al., 1993; Barrett et al., 1994; Basserman, 1997; Dongarra et al., 1998), most of them have dealt with preconditioners based on incomplete factorization techniques. These techniques are very inefficient in a parallel computer environment (Dongarra et al., 1991) if a natural ordering of the matrix is employed. However, some works do show that a suitable reordering of the matrices can result in efficient parallel implementations of incomplete factorization techniques (Jones and

Plassmann, 1993). There have been other studies (Chronopoulos and Gear, 1989; Aykanat et al., 1990) which have been focused on the parallel implementation of the unpreconditioned conjugate gradient (CG) method. In this work, the most widely used Jacobi-like preconditioners have been implemented.

The parallelization of the Krylov subspace technique method is rather simple, since every vector operation of this algorithm can be parallelized separately; that is, each processor executes scalar operations on a subset or domain of the components of a vector and a block partition of the vectors suffices to obtain good performance. For problems derived from the finite discretization of partial differential equations on three-dimensional regular/structured grids, the block partition of the system matrix by rows and its corresponding aligned vectors are equivalent to a block partition of grid points in one of the spatial directions if a natural ordering of grid points is employed. In our approach, no partition has been used because of the use of unstructured grids.

7.4.1. Parallel Krylov subspace methods

In this section, we describe an iterative linear system solution methodology used for the parallel unstructured finite volume simulation of the strongly coupled fluid flow, heat transfer, and mass transfer that occur in volcanic eruption plumes. The nonlinear/linear iterative solution strategies are based on a fully coupled Newton solver with preconditioned Krylov subspace methods as the underlying linear iteration. Our discussion considers computational efficiency, robustness, and a number of practical implementation issues. The evaluated preconditioners are based on additive Schwarz DD methods which are applicable for totally unstructured meshes. A number of different aspects of Schwarz schemes are considered, including subdomain solves, use of overlap, and the introduction of a coarse grid solve (a two-level scheme). As we will show, the proper choice among DD options is often critical to the efficiency of the overall solution scheme.

As noted on several occasions, simulations of volcanic plumes require the solution of strongly coupled interacting physics in complex three-dimensional geometries with high-resolution unstructured meshes to capture all relevant length scales. After suitable spatial (finite volume) discretization and linearization, these simulations produce large linear systems of equations with a huge number of unknowns. As a result, efficient and robust parallel iterative solution methods are required to make such simulations possible. Preconditioned Krylov iterative methods are among the most robust and fastest iterative solvers over a wide variety of CFD applications.

In the last decade, there has been a significant amount of work on parallel Krylov methods, and a number of general purpose Krylov solver libraries have been developed. In general, these Krylov methods are relatively straightforward to implement, highly parallel, and are often 'optimal' in some sense. While the convergence characteristics of specific Krylov methods remains a topic of research interest, it is now clear that the key factor influencing the robustness and efficiency of these solution methods is preconditioning.

Since volcanic eruption clouds are characterized by both locally elliptic and nearly hyperbolic behavior, localized steep gradients, and often strongly coupled interactions between the gaseous and particulate phases, there is a strong coupling between the governing partial differential equations. The nonlinear algebraic equations that result from the discretization of these equations may be solved robustly and efficiently by means of preconditioned Krylov subspace methods. The preconditioners considered here fall into the family of Schwarz DD methods. These schemes partition the original domain into subdomains and approximately solve the discrete problems corresponding to the individual subdomains in parallel.

Among Schwarz schemes, there are a number of choices which can greatly affect the overall solution time and robustness. These choices include the subdomain size, the amount of overlap between subdomains, and the partitioning metric which can alter the shape and aspect ratios of subdomains. The choices also include the selection of subdomain solvers, such as an incomplete lower–upper (ILU) factorization (with further options for dropping nonzeros in the factorizations and ordering equations within a subdomain) and the introduction of a coarse grid solve. Among these issues, the proper choice among DD options is often critical to the efficiency of the overall solution scheme.

A finite-volume discretization of our partial differential equations gives rise to a system of coupled, nonlinear, nonsymmetric algebraic equations, the numerical solution of which is very challenging. These equations are linearized using an inexact form of Newton method, with the block matrix representation of these discrete linearized equations written as

$$\begin{pmatrix} A & -B^T \\ BR & K \end{pmatrix} \begin{pmatrix} \phi \\ p \end{pmatrix} = \begin{pmatrix} F_\phi \\ F_p \end{pmatrix} \tag{7.59}$$

where the block diagonal contribution has been highlighted by a specific ordering.

In this representation, the vector ϕ contains the Newton updates to all the dependent variables with the exception of pressures p. The block matrix A corresponds to the combined discrete convection, diffusion, and source operators for all the unknowns. The matrix B corresponds to the discrete divergence operator with its transpose the gradient operator. The diagonal matrix R results from the expansion of density and velocity, and the matrix K corresponds to the discrete 'pressure Laplacian' operator. This pressure operator corresponds to the discretization of Poisson equation that results from taking the divergence of the momentum equations presented in Section 7.2, while the vectors F_ϕ and F_p contain the right-hand side residuals for Newton method.

The existence of the well-conditioned nonzero matrix K allows the solution of the linear systems with a number of algebraic and DD type preconditioners. This is in contrast to other formulations, such as Galerkin finite element methods that use mixed interpolation and result in a zero block on the total mass continuity diagonal. The difficulty of producing robust and efficient preconditioners for the Galerkin finite element formulation has motivated the use of many different types of solution methodologies.

In the approach proposed here, the full coupling of partial differential equations in the nonlinear solver preserves the inherently strong coupling of the physics with the goal of producing a robust solution methodology. The preservation of this strong coupling places, however, a significant burden on the linear solution procedure to solve the fully coupled algebraic system, as we will show below.

The Newton–Krylov method is an implementation of Newton method in which a Krylov iterative solution technique is used to approximately solve the linear systems that are generated at each step of Newton method. Specifically, to solve the nonlinear system $F(x) = 0$, we seek a zero of $F \in \Re^n$, where $x \in \Re^n$ is a current approximate solution. The Krylov iterative solver is applied to determine an approximate solution of the Newton equation $J(x)s = -F(x)$, where $J(x)$ is the Jacobian matrix of F at x. The Newton–Krylov method is usually implemented as an inexact Newton method (Eisenstat and Walker, 1994; Shadid et al., 1997) for approximately solving $J(x)s = -F(x)$. One chooses a forcing term $\eta \in [0, 1)$ and then applies Krylov method until an iterate s_k satisfies the inexact Newton condition

$$||F(x) + J(x)s_k|| \leqslant \eta ||F(x)|| \tag{7.60}$$

One would assume that, in the initial stages of the Newton iteration, when the current approximation is far from the true solution, there would be no benefit from solving too accurately the Newton equations with the inaccurate Jacobian matrix $J(x_k)$ that is currently available. Normally, our inexact Newton method formulation uses an adaptive convergence criteria to reduce the amount of over-solving that occurs and to produce a more computationally efficient nonlinear solution procedure. To improve robustness, a back-tracking algorithm can be used. This globalization method selects an update vector s_k by scaling a Newton step as needed to ensure that the nonlinear residual has been reduced adequately before the step is accepted.

It is worth noting that there are two related issues in the solution of nonlinear equations that result from the finite volume discretization of partial differential equations. The first is associated with the nonlinear Newton methods and the second with the solution of the linear systems by preconditioned Krylov methods.

The linear subproblems generated from the inexact Newton method are solved by preconditioned Krylov methods which include the restarted generalized minimal residual GMRES(k) and transpose-free quasi-minimal residual techniques for nonsymmetric systems. All Krylov methods rely on a small, but well defined set of basic kernel routines that consist of parallel matrix–vector, vector–vector, vector inner–product, and preconditioning operations.

It is well known that the overall performance of Krylov methods can be substantially improved when one uses preconditioning (Saad and Schultz, 1986; Saad, 1989, 2003). The basic idea is that instead of solving the system $Ax = b$, the system $AM^{-1}y = b$ is solved instead, where M^{-1} is an approximation to A^{-1} that is easily computed. Since only matrix–vector products are needed, it is not necessary to form explicitly AM^{-1}; that is, only good software is needed to solve $Mv = y$. We note that the preconditioning described here corresponds to 'right' preconditioning, for

it is also possible to precondition on the 'left', that is, $M^{-1}A$. Here, we only consider right preconditioning, because, when left preconditioning is used, the computed residual corresponds to a preconditioned residual. If convergence is thus based on the size of the residual, changing the preconditioner effectively changes the convergence criteria.

The preconditioners that are considered are based on algebraic additive Schwarz DD preconditioners with variable overlapping between subdomains, although other preconditioners such as Jacobi, block—Jacobi, and polynomial expansions can also be considered.

A formal description of the variable overlap additive Schwarz preconditioner can be described by considering the linear system $Ax = b$, where A is an $n \times n$ nonsymmetric matrix, with the matrix entry in the ith row and jth column given by a_{ij}. This matrix induces a directed graph which can be defined in the following way. Each row of A corresponds to a vertex and each $a_{ij} \neq 0$ corresponds to an edge incident from node i to j. We denote the set of graph vertices by $V(A)$ and similarly the set of edges by $E(A)$. Throughout the rest of this discussion, the argument A in $V(A)$ and $E(A)$ will be dropped to facilitate the presentation. The set of edges and vertices defines a matrix graph $G(V, E)$.

Domain decomposition methods rely on approximate solutions on subdomains. These subdomains are defined in terms of vertex subsets. To discuss vertex subsets we use the notation to denote by V_k^i the kth subdomain in an i-overlap method. Assume that $V_k{}^i$ is defined and corresponds to a subset of vertices. The following edge set can then be associated with the vertex subset

$$E_k^i = \{e_i = (x, y) \in E \mid x \in V_k^i, y \in V\} \tag{7.61}$$

where E_k^i includes all the edges emanating from V_k^i.

To complete the definition of the Schwarz method, we must now define the vertex subsets. Assume that the vertices have been partitioned into p disjoint sets V_i^0, such that $V = \bigcup_{i=1}^p V_i^0$ and $V_i^0 \cap V_j^0 = 0$ for $i \neq j$. This vertex partitioning corresponds to the distribution of the matrix over the processors and effectively defines the 0th overlap subdomains. To define the kth overlap subdomains, we use the edge sets associated with the $(k-1)$th overlap subdomains

$$V_k^i = \{x \in V \mid \exists y \in V, (x, y) \text{ or } (y, x) \in E_k^{i-1}\} \tag{7.62}$$

To define overlap in an ith overlap additive Schwarz method, we use the vertex sets V_k^i. Specifically, consider the restriction matrix I_k^i of size $m \times n$, where m is the number of nodes in V_k^i, n is the total number of nodes in V, and $I_k^i(l, 1) = 1$ if j is the lth node in V_k^i and $I_k^i(l, 1) = 0$ otherwise, for $1 \leqslant k \leqslant p$. The $I_k{}^i$ operators essentially map the entire space to the kth subdomain. The ith overlap additive Schwarz preconditioner is now given by

$$M^{-1} = \sum_{k=1}^{p} I_k^i \left((I_k^i)^T A I_k^i\right)^{-1} (I_k^i)^T \tag{7.63}$$

This method corresponds to projecting the equations onto a series of overlapping subdomains defined by the vertex sets and solving each subsystem. Since these subdomain solves are independent, they can be performed concurrently. In this manner, the overlapping can be viewed as a means to increase robustness by expanding individual subdomains to include finite volumes or nodes assigned to neighboring processors by allowing more coupling between subdomains (or processors). In a geometric sense, this overlap corresponds to increasing the size of the locally defined subdomain to include additional levels of finite volumes or nodes outside of the processors-assigned nodes. Thus, a single level of overlapping uses only the information from finite volumes that are connected by an edge in the connectivity graph that was cut by the original subdomain partition. Successive levels of overlap now use this method recursively by considering the previously overlapped points to be assigned nodes to the subdomain.

This method can be referred to as a one-level scheme. A two-level scheme uses not only the fine grid operator defined above, but also adds an additional projection of the original equations onto a coarser grid. This two-level DD method is given by

$$M^{-1} = \sum_{k=0}^{p} I_k^i ((I_k^i)^T A I_k^i)^{-1} (I_k^i)^T \tag{7.64}$$

where I_0^i is an interpolation operator that maps solution vectors from the original mesh to an auxiliary coarser mesh that covers the same domain as the original one, but with significantly fewer grid points. Theoretically, the number of mesh points should be about the same size as the number of subdomains. When A is a symmetric positive definite discrete elliptic operator and a sufficient amount of overlap is used, the convergence of the iterative method using a DD preconditioner is independent of the number of unknowns in the matrix. In cases where a more modest overlap is used, the theoretical convergence depends mildly on the size of the subdomains. In the case where A is nonsymmetric, much less is known about the convergence of this technique for coupled systems of partial differential equations. It is important to notice that, with the addition of the coarse grid solve, the DD method is no longer completely algebraic.

While a direct factorization could be used on the subdomains, our experience indicates that this is rarely practical as the storage and time associated with this direct factorization is too high. Instead of solving the submatrix systems exactly, we use an incomplete factorization technique on each subdomain (or processor). Here, we employ two specific ILU factorizations: The standard ILU(0) method with no fill-in as well as the ILUT (fill-in, drop) incomplete factorization which allows specification of a user-specified fill-in parameter (fill-in 1.0) and a drop tolerance. In this nomenclature, a fill-in of 1.5 denotes an ILU factor with up to 1.5 times as many nonzeros as the original matrix.

It is important to remark that the partitioning of mesh into subdomains and that the subdomain-to-processor assignments are not trivial tasks, for both the partitions and the subdomain mappings have to be performed in order to achieve low communication volume, good load balance, few message start-ups, and only small amounts of network congestion.

7.4.2. Ordering of algebraic equations

Since the finite volume discretization of a system of n_e partial differential equations in each subdomain or block results in $n_e \times n_x \times n_y \times n_z$ nodal variables and algebraic equations, a main issue when solving systems of algebraic equations is the ordering of equations and variables. A natural ordering of grid points and blocking of nodal variables has been chosen here because of its better cache behavior.

As indicated above, in order to solve the system $\mathbf{Ax} = \mathbf{b}$ the Krylov subspace method (Saad, 2003) has been used (Barrett et al., 1994), although the BiCGStab technique could also be used. The Krylov subspace method is an iterative technique which converges to the exact solution in exact arithmetic, through a sequence of n vector approximations, where $n = n_e \times n_x \times n_y \times n_z$ is the dimension of both $\mathbf{x}$ and $\mathbf{b}$. From any vector approximation to the solution, a search direction which is conjugate to the previous ones is used to determine a new approximation. In practice, only few iterations are employed to obtain a good estimate of the solution. In the preconditioned version of the Krylov subspace method, both the condition number of $\mathbf{A}$ and the number of iterations may be reduced by pre-multiplying the system $\mathbf{Ax} = \mathbf{b}$ by a preconditioner, which is usually the inverse of an approximation to $\mathbf{A}$. It should be noted that some authors call preconditioner to the approximation itself.

Jacobi, block–Jacobi, incomplete Cholesky, and incomplete-block Cholesky preconditioners can be tested (Barrett et al., 1994). For block-based preconditioners, however, the N dependent variables per node can be used to form $N \times N$ blocks. Our experience indicates that the Jacobi preconditioner is the most efficient one for three-dimensional reaction–diffusion equations (Ortigosa et al., 2001, 2003).

7.4.3. Matrix–vector products

Each iteration of the preconditioned Krylov subspace method contains inner and sparse matrix vector products, and, therefore, requires at least three communication steps and their corresponding synchronizations. Note that the saxpy $(\alpha\mathbf{x} + \mathbf{y})$ operations do not require inter-processor communications. A reorganization of computations in the preconditioned Krylov subspace method can be implemented in order to hide the latency of communications. This overlap of communications with computations can be implemented by using asynchronous messages in the message-passing interface (MPI) model and prefetch directives on a shared-memory (SM) environment.

The parallelization of the product $\mathbf{q} = \mathbf{Ap}$ in the preconditioned Krylov subspace method for banded matrices can be performed with a nearly perfect overlap between the messages and computations in many cases (Romero and Zapata, 1995; Basserman, 1997). The required message with the halo data of $\mathbf{p}$ (the data corresponding to the grid points in the domain of one processor that are used to compute the data of $\mathbf{q}$ in a neighboring processor) is overlapped with computations of matrix rows corresponding to the inner part of the domain, where the inner part is the domain without its halos. For a block distribution along the vertical axis, overlapping is possible if the halos on both sides of the processor domain do not overlap. For general banded matrices, the overlap can be partially achieved if the

number of rows assigned to a processor is, at least, twice the matrix bandwidth. The latency of the communication step in the inner product $\mathbf{p}^T \cdot \mathbf{q}$ can be hidden by delaying the update of $\mathbf{x}_i$ by one iteration. For the inner product $\mathbf{r}^T \cdot \mathbf{z}$, a solution which hides the latency has been proposed by Demmel et al. (1993) where an incomplete factorization is employed as preconditioner.

As indicated above, our work adopts a parallelization strategy for the numerical simulations based on a geometric DD and the single program multiple data (SPMD) programming paradigm (Tai and Zhao, 2003). Here, the communication of data between domains is based on the message-passing interface (MPI) (Gropp et al., 1994).

Domain decomposition of a mesh into a set of sub-domains that may be allocated to a set of processors involves finding a partition of the mesh so that each processor utilizes an equal amount of computational time. The nodes and control volumes/elements that are allocated uniquely to a processor are referred to as core mesh components in this work, with each processor having the task of calculating the flow field variables and nodal gradients for these components. Note that in the overlapping DD described above, the overlapping domains can be considered as the union of non-overlapping domains and overlapping layers. Therefore, each overlapping sub-domain can be considered as a non-overlapping one that is enclosed with a layer of ghost nodes and overlapping elements, which overlap the sub-domains along the inter-processor boundaries. These ghost nodes store flow field variables and nodal gradients, which are transferred from neighboring sub-domains for the solution of variables within the sub-domain. Communication between these core and ghost nodes is based on MPI. The data flow direction is always from the core nodes to the ghost nodes.

7.4.4. Programming paradigms

Although we described the MPI, one can also consider other programming paradigms, such as the SM programming model (OpenMP, 1997) and two message-passing paradigms (MPI-1, 1994; MPI-2, 1997; and SHMEM, 1994). The synchronization points required for inner products can be implemented by using counters protected by lock variables. Additional flags can be included in order to grant permission for accessing halo data. As soon as a processor has computed the data on its borders, it enables the flag. If another processor requires these data, it waits for this flag to be enabled. Reset of counters and flags can be carefully implemented by means of odd and even sense-reversing flags to enhance performance and avoid data race conditions.

In the message-passing version, MPI-1 and SHMEM libraries can be considered because of their better efficiencies in many computer architectures. MPI-1 libraries have been widely adopted as the message-passing interface of choice for many years. In this implementation, the inter-processor communication is performed through a special routine *send* that sends a message and a matching routine *receive* that receives a message. When using MPI-1 libraries, the waits for the arrivals of messages imply a synchronization by themselves.

On the other hand, SHMEM libraries provide single-sided communication routines in which any processor can *put* a data package on a remote memory, or it could *get* data stored there. When using SHMEM libraries, *shmem_put* is to be preferred over *shmem_get* because it allows communication overlapping, although the cache miss rate increases. Additional messages with flags can be added as in the OpenMP implementation for synchronization purposes if the computer architectures used ensure that the arrivals of messages keep the same order as that of their departures.

In both shared-memory and message-passing paradigms, global barriers should be avoided because, when a global barrier is used, each processor must wait until the others finish their computations in order to continue with its own computations at the same point of the code. In addition, it is more efficient that a processor requiring data in a point of the code ('waiting point') uses the data generated by other processors at a previous point of the code ('permission point').

7.4.5. Computer architectures

Our experience has been centered so far on the following computer architectures:

- Cray T3E-900. A massively parallel processor (MPP) with 400 MHz DEC Alpha–EV5.6 processors. For this architecture, the vendor supplies the message-passing programming models MPI and SHMEM.
- Origin2000. A cache-coherent, non-uniform memory access architecture with 400 MHz MIPS–R12000 processors. For this architecture, the vendor supplies OpenMP, MPI, and SHMEM.
- Sun HPC6500. A uniform-memory access, symmetric multiprocessor system with 400 MHz UltraSPARC–II processors. For this architecture, the vendor supplies MPI and OpenMP.

The availability of cluster or distributed computing with OpenMP may offer advantages over the above computer architectures in terms of cost, availability, etc. For three-dimensional simulations of highly nonlinear reaction–diffusion equations exhibiting steep gradients and high temporal derivatives and two-dimensional simulations of compressible chemically reacting flows in both confined and unconfined geometries, our experience of efficient parallel implementation of the Krylov subspace method indicates that:

- Optimized BLAS libraries for each architecture should be employed because they are more efficient than the ones developed by the users. In particular, the SciLib, Sun Performance Library (sunperf), and sgimath libraries should be employed in the Cray, Sun, and Origin2000 computers, respectively.
- The choice of a programming model depends on the problem size and the computer architecture used.
- The overlap in the matrix–vector product and the delay update of the $\mathbf{x}$-vector do not improve much the performance of message-passing models.
- Memory access overlap should be used, but without losing locality.
- The ordered versions of the code with overlap significantly improve the efficiency of OpenMP codes.

- The inclusion of cache prefetching directives which are available in most recent architectures allows for data access on the highest level of hierarchy of the local memory, while other computations are being performed.
- A reduction in the number of synchronization points does not improve the load imbalance.
- Locality should be increased to the highest possible level.
- Machine-specific libraries (such as saxpy) are preferred.
- The computation reordering penalizes the cache performance.

Based on this experience, a good scheduling of operations should maintain the computations in the same order as in the original algorithm; that is, every vector should be computed as near as possible to the operation where it is, required. In addition, a maximum exploitation of the locality of data and an overlap of halo messages with computations should be used, because they represent a large fraction of calculations.

7.5. CONCLUSION

In this chapter, we have summarized our research efforts on the physical modeling, numerical solution, and computer implementation methodologies for the effective, reliable and accurate simulations of volcanic eruption columns. Volcanic plumes involve complex interactions between the material emitted from the volcano and the atmosphere into which this material is discharged. The erupted material consists of both volcanic gases and volatiles, and different size pyroclasts that result in gas–gas, gas–particle, and particle–particle interactions in the atmosphere. Typical processes within a plume include condensation and evaporation of volatiles, fragmentation and aggregation of particulates, growth of aerosols and fine ash particulates into water droplets that produce precipitation, and chemical reactions between the volcanic and atmospheric constituents.

Global scale dynamics and thermodynamics of volcanic plumes cascades the turbulent energy down to small scales where this energy is dissipated through the interaction with local microphysical processes. This interaction, in turn, modifies the global scale processes within the plume. Turbulence is ubiquitous in volcanic plumes and presents modeling problems, because the small scales cannot be adequately resolved with today's technology and must be, therefore, properly modeled. Since existing pyroclastic dispersion models do not account accurately for the two-way coupling between the gaseous and particulate matter, we have developed a new model that does account for such a coupling in a more physically satisfactory manner.

This model is based on volume averaging of single-phase transport laws for the conservation of mass, momentum, and energy, and on taking moments of these equations with respect to the center of mass of the averaging volume. The averaged form of transport equations accounts for both the mean motion and properties of each phase in the averaging volume and the structural or local effects within this volume. These structural properties consist of phase inertia and contraction/expansion or dilatancy effects, and thus account for small scales which are commonly modeled through subgrid scale turbulence models. The small scale effects are modeled

with an additional set of transport equations. The model also accounts for a yield-type behavior of the material when the particulate concentration gradients become high. We have also presented some closure or constitutive relations for an arbitrary number of phases undergoing mass, momentum, and energy exchanges, and additional mass transport equations for modeling multicomponent multiphase mixtures with phase change and chemical reactions. The modeling approach presented here uses both the Eulerian and Lagrangian frameworks, depending on the size of particles. The resulting modeling equations can be transformed into conservation-law form which is suitable for implementation with different numerical techniques.

The discretization of the Eulerian phases has been performed using a domain decomposition technique in a multiblock grid consisting of hexahedra and tetrahedra, a conservative finite volume formulation, and implicit, first- and second-order accurate discretizations of time derivatives. The multiblock technique allows to design grids that are adapted to the terrain topography and add and remove finite volumes in the leeward and windward sides, respectively, of the pyroclastic plume when there are crosswind effects. The discretization of the advective terms in the Eulerian phase equations is based on a weighted essentially non-oscillatory method that is second-order accurate in regions with steep gradients of flow variables, and third-order accurate in smooth regions.

Two different approaches have been followed in the time discretization of the Lagrangian phase equations. The first uses time linearization and results in linear algebraic equations at each time level that are solved by means of the biconjugate gradient-stabilized method for nonsymmetric matrices in each subdomain or block. This technique, however, does not provide acceptable results when either the time step or the duration of a volcanic eruption are large due to the accumulation of temporal truncation errors. For this reason, a second method for solving the nonlinear algebraic equations that result from the space and time discretizations of governing equations in each domain is proposed. This method uses an inexact Newton method and the resulting linear equations at each iteration are solved by means of a Krylov subspace method that uses algebraic domain decomposition and an incomplete lower-upper factorization preconditioner.

Due to the spatial and temporal characteristics of volcanic eruptions, an accurate simulation of the modeling equations is a rather demanding task. This requires the use of advanced parallel computer paradigms that take into consideration the computer architecture, the synchronization of messages, and the processors' latency and lag times. Our experience has so far been centered on massively parallel processors, cache-coherent, nonuniform access computer architectures, and symmetric multiprocessors with both OpenMP and MPI. This experience has shown that, amongst other considerations, the overlap in matrix–vector products does not improve much the performance of message-passing models, memory access overlap should be used without losing locality, locality should be increased to the highest possible level, ordered versions of the code with overlap significantly improve the efficiency of OpenMP codes, and inclusion of cache prefetching directives allows for data access on the highest level of hierarchy of the local memory while other computations are being performed.

Following an extensive verification stage involving the assessment of the accuracy and efficiency of different numerical solvers, number of phases, and phase interactions, we will begin validating the pyroclastic dispersion model. After that, we will ascertain that the predictions of the model reproduce the behavior of some key eruption columns, including those of Vesuvius. Once our verification and validation studies are completed, the pyroclastic flow model described in this chapter will be integrated with our magma chamber dynamics, opening of volcanic conduits, and magma ascent models into a simulation package or Global Volcanic Simulator. As discussed in Chapter 1, the objective of such a simulator is to assess the effects of different eruption scenarios on the territory surrounding Vesuvius, for the purpose of developing a more secure habitat for over one million people living in the close proximity of this volcano.

REFERENCES

AGU, 1992. Volcanism and Climate Change. American Geophysical Union, Washington, DC.

Ahmadi, G. and Ma, D., 1990. A thermodynamical formulation for dispersed multiphase turbulent flows I. Int. J. Multiphase Flow, 16: 323–340.

Ammann, M. and Burtscher, H., 1993. Aerosol dynamics and light-scattering properties of a volcanic plume. J. Geophys. Res., 98: 19705–19711.

Aykanat, C., Özgüner, F. and Scott, D.S., 1990. Vectorization and parallelization of the conjugate gradient algorithm on hypercube-connected vector processors. Microprocess. Microprog., 29: 67–82.

Barrett, R., Berry, M., Chan, T.F., Demmel, J., Donato, J., Dongarra, J., Eijkhout, V., Pozo, R., Romine, C. and Van de Vorst, H., 1994. Templates for the Solution of Linear Systems: Building Blocks for Iterative Methods. SIAM, Philadelphia.

Basserman, A., 1997. Parallel sparse matrix computations in iterative solvers on distributed memory machines. J. Parallel Distrib. Comput., 45: 46–52.

Blake, S., 2003. Correlation between eruption magnitude, SO_2 yield, and surface cooling. In: C. Oppenheimer, D.M. Pyle and J. Barclay (Eds), Volcanic Degassing. The Geological Society, London, pp. 371–380.

Bowen, R., 1976. Theory of mixtures. In: A.C. Eringen (Ed.), Continuum Physics III. Academic Press, New York, pp. 1–127.

Brasseur, G. and Granier, C., 1992. Mount Pinatubo aerosols, chlorofluorocarbons, and ozone depletion. Science, 257: 1239–1242.

Brazier, S., Sparks, R.S.J., Carey, S.N., Sigurdsson, H. and Westgate, J.A., 1983. Bimodal grain size distribution and secondary thickening in air-fall ash layers. Nature, 301: 115–119.

Brown, P.N. and Saad, Y., 1990. Hybrid Krylov methods for nonlinear systems of equations. SIAM J. Sci. Stat. Comput., 11: 450–481.

Carey, S.N. and Sigurdsson, H., 1982. Influence of particle aggregation on deposition of distal tephra from the May 18, 1980, eruption of Mount St. Helens volcano. J. Geophys. Res., 87: 7061–7072.

Cas, R.A.F. and Wright, J.V., 1993. Volcanic Successions. Unwin, London.
Charlson, R.J., Seinfeld, J.H., Nenes, A., Kulmala, M., Laaksonen, A. and Facchini, M.C., 2001. Reshaping the theory of cloud formation. Science, 292: 2025–2026.
Cheney, W. and Kincaid, D., 2004. Numerical Mathematics and Computing. Thompson/Brooks/Cole, New York.
Chesshire, G. and Henshaw, W.D., 1990. Composite overlapping meshes for the solution of partial differential equations. J. Comput. Phys., 90: 1–64.
Chronopoulos, A.T. and Gear, C.W., 1989. S-step iterative methods for symmetric linear systems. J. Comput. Appl. Math., 25: 153–168.
Cioni, R., Marianelli, P. and Sbrana, A., 1992. Dynamics of the A.D. 79 eruption: Stratigraphic, sedimentological and geochemical data on the successions from the Somma–Vesuvius southern and eastern sectors. Acta Vulcanol., 2: 109–123.
Coniglio, S. and Dobran, F., 1995. Simulations of magma ascent and pyroclast dispersal at Vulcano (Aeolian Islands, Italy). J. Volcanol. Geotherm. Res., 65: 297–317.
Crowe, C.T., 1982. Review – numerical models for dilute gas-particle flows. J. Fluid. Eng., 104: 297–303.
Dartevelle, S., 2004. Numerical modeling of geophysical granular flows: 1. A comprehensive approach to granular rheologies and geophysical multiphase flows. Geochem. Geophys. Geosyst., 5: 10.1029/2003GC000636, 1–28.
Dartevelle, S., Rose, W.I., Stix, J., Kelfoun, K. and Vallance, J.W., 2004. Numerical modeling of geophysical granular flows: 2. Computer simulations of plinian clouds and pyroclastic flows and surges. Geochem. Geophys. Geosyst., 5: 10.1029/2003GC000637, 1–36.
Darwish, M., Moukalled, F. and Sekar, B., 2001. A unified formulation of the segregated class of algorithms for multifluid flow at all speeds. Numer. Heat Transfer, Part B, 40: 99–137.
Davidson, P.A., 2004. Turbulence. Oxford University Press, Cambridge.
Demkowicz, L., Devloo, Ph. and Oden, J.T., 1985. On an h-type mesh-refinement strategy based on minimization of interpolation errors. Comput. Meth. Appl. Mech. Eng., 53: 67–89.
Demmel, J., Heath, M. and van der Vorst, H., 1993. Parallel linear algebra. Acta Numerica, 2: 111–197.
Dobran, F., 1991. Theory of Structured Multiphase Mixtures. Springer-Verlag (Springer), New York.
Dobran, F., 1992. Modeling of structured multiphase mixtures. Int. J. Eng. Sci., 30: 1497–1505.
Dobran, F., 1993. Global Volcanic Simulation of Vesuvius. Giardini, Pisa.
Dobran, F., 1994a. Prospects for the global volcanic simulation of Vesuvius. Accademia Nazionale dei Lincei, 112: 197–209.
Dobran, F., 1994b. Incontro con il Vesuvio, Sapere, November: 11–16
Dobran, F., 1994b. ETNA: Magma and Lava Flow Modeling and Volcanic System Definition Aimed at Hazard Assessment. GVES, Rome.
Dobran, F., 2001. Volcanic Processes: Mechanisms in Material Transport. Kluwer Academic/Plenum Publishers (Springer), New York.

Dobran, F., 2006. VESUVIUS 2000: Toward Security and Prosperity Under the Shadow of Vesuvius. This volume (Chapter 1).

Dobran, F. and Coniglio, S., 1996. Magma ascent simulations of Etna's eruptions aimed at internal system definition. J. Geophys. Res., 101: 713–731.

Dobran, F. and Hur, N., 1990. Turbulence modeling and distribution in phases in an annular two-phase flow. In: T.N. Veziroglu (Ed.), Multiphase Transport and Particulate Phenomena. Hemisphere Publishing Corporation, New York, pp. 25–61.

Dobran, F. and Luongo, G., 1995. VESUVIUS 2000: Project Summary and Field Work. GVES, Rome.

Dobran, F. and Mulargia, F., 1991. Prospects for the Simulation of Volcanic Eruptions. Giardini, Pisa.

Dobran, F. and Papale, P., 1993. Magma–water interaction in closed systems and application to lava tunnels and volcanic conduits. J. Geophys. Res., 98: 14041–14058.

Dobran, F., Barberi, F. and Casarosa, C., 1991. Modeling of Volcanic Eruptions. Giardini, Pisa.

Dobran, F., Neri, A. and Macedonio, G., 1993. Numerical simulation of collapsing volcanic columns. J. Geophys. Res., 98: 4231–4259.

Dobran, F., Neri, A. and Todesco, M., 1994. Assessing the pyroclastic flow hazard at Vesuvius. Nature, 367: 551–554.

Dominé, F. and Thibert, E., 1996. Mechanism of incorporation of trace gases in ice grown from the gas phase. Geophys. Res. Lett., 23: 3627–3630.

Dongarra, J., Duff, I., Sorensen, D. and van der Vorst, H., 1991. Solving Linear Systems on Vector and Shared Memory Computers. SIAM, Philadelphia.

Dongarra, J., Duff, I., Sorensen, D. and van der Vorst, H., 1998. Numerical Linear Algebra for High-Performance Computers. SIAM, Philadelphia.

Drew, D.A. and Passman, S.L., 1999. Theory of Multicomponent Fluids. Springer, New York.

Eaton, J.K. and Fessler, J.R., 1994. Preferential concentration of particles by turbulence. Int. J. Multiphase Flow, 20: 169–209.

Eiseman, P.R., 1985. Alternating direction adaptive grid generation. AIAA J., 23: 551–560.

Eisenstat, S.C. and Walker, H.F., 1994. Globally convergent inexact Newton methods. SIAM J. Optim., 4: 393–422.

Elghobashi, S.E. and Abou-Arab, T.W., 1983. A two-equation turbulence model for two-phase flows. Phys. Fluids, 26: 931–938.

Eriksson, L.E., 1982. Generation of boundary-conforming grids around wing-body configurations using transfinite interpolation. AIAA J., 20: 1313–1320.

Esposti Ongaro, T., Neri, A., Todesco, M. and Macedonio, G., 2002. A pyroclastic flow hazard at Vesuvius from numerical modeling: 2. Analysis of local flow variables. Bull. Volcanol., 64: 178–191.

Ferziger, J.H., 1993. Subgrid-scale modeling. In: B. Galperin and S.A. Orszag (Eds), Large Eddy Simulation of Complex Engineering and Geophysical Flows. Cambridge University Press, Cambridge, pp. 37–54.

Frey, P.J. and George, P.L., 1999. Maillages. Hermes, Paris.

Gelbard, F. and Seinfeld, J.H., 1979. The general dynamic equation for aerosols – theory and application to aerosol formation and growth. J. Colloid Interface Sci., 68: 363–382.

George, P.L. and Borouchaki, H., 1998. Delaunay Triangulation and Meshing. Hermes, Paris.

Giordano, G. and Dobran, F., 1994. Computer simulations of the Tuscolano Artemisio's second pyroclastic flow unit (Alban Hills, Latium, Italy). J. Volcanol. Geotherm. Res., 61: 69–94.

Glaze, L.S., Baloga, S.M. and Wilson, L., 1997. Transport of atmospheric water vapour by volcanic eruption columns. J. Geophys. Res., 102: 6099–6108.

Graf, H.F., 2004. The complex interaction of aerosols and clouds. Science, 303: 1309–1311.

Graf, H.F., Herzog, M., Oberhuber, J.M. and Textor, C., 1999. The effect of environmental conditions on volcanic plume rise. J. Geophys. Res., 104: 24309–24320.

Goodman, M.A. and Cowin, S.C., 1972. A continuum theory for granular materials. Arch. Rat. Mech. Anal., 44: 249–266.

Gropp, W., Lusk, E. and Skjellum, A., 1994. Using MPI: Portable Parallel Programming with the Message-Passing Interface. MIT Press, Cambridge.

Herzog, M., Graf, H.F., Textor, C. and Oberhuber, J.M., 1998. The effect of phase changes of water on the development of volcanic plumes. J. Volcanol. Geotherm. Res., 87: 55–74.

Hirschfelder, J.O., Curtiss, C.F. and Bird, R.B., 1954. Molecular Theory of Gases and Liquids. Wiley, New York.

Hobbs, P.V., Tuell, J.P., Hegg, D.A., Radke, L.F. and Eltgroth, M.W., 1982. Particles and gases in the emissions from the 1980–1981 volcanic eruptions of Mt. St. Helens. J. Geophys. Res., 87: 11062–11086.

Isaacson, E. and Keller, H.B., 1966. Analysis of Numerical Methods. Wiley, New York.

Ishii, M., 1975. Thermo-Fluid Dynamic Theory of Two Phase Flows. Eyrolles, Paris.

Jiang, G.-S. and Shu, C.-W., 1996. Efficient implementation of weighted ENO schemes. J. Comput. Phys., 126: 202–228.

Jones, M.T. and Plassmann, P.E., 1993. A parallel graph coloring heuristic. SIAM J. Sci. Stat. Comput., 14: 654–669.

Kallinderis, Y., Khawaja, A. and McMorris, H., 1996. Hybrid prismatic/tetrahedral grid generation for viscous flows around complex geometries. AIAA J., 34: 291–298.

Kim, J., Kim, D. and Choi, H., 2001. An immersed boundary finite-volume method for simulations of flow in complex geometries. J. Comput. Phys., 171: 132–150.

Knoll, D.A. and McHugh, P.R., 1995. Newton–Krylov methods applied to a system of convection–diffusion—reaction equations. Comput. Phys. Commun., 88: 141–160.

Koop, T., 2000. The formation of ice clouds from supercooled aqueous aerosols. In: B.N. Hale and M. Kulmala (Eds), Nucleation and Atmospheric Aerosols 2000. American Institute of Physics, Melville, pp. 549–560.

Laaksonen, A., 2000. Application of nucleation theories to atmospheric aerosol formation. In: B.N. Hale and M. Kulmala (Eds), Nucleation and Atmospheric Aerosols 2000. American Institute of Physics, Melville, pp. 711–723.

Leonard, B. and Mokhtari, S., 1990. Beyond first-order upwinding: The ultra sharp alternative for non-oscillatory steady-state simulation of convection. Int. J. Numer. Method. Eng., 30: 729–766.

Luhr, J.F., 1991. Volcanic shade causes cooling. Nature, 354: 104–105.

Macedonio, G., Dobran, F. and Neri, A., 1994. Erosion processes in volcanic conduits and application to the AD 79 eruption of Vesuvius. Earth Planet. Sci. Lett., 121: 137–152.

Mather, T.A., Pyle, D.M. and Oppenheimer, C., 2003. Tropospheric volcanic aerosol. In: A. Robock and C. Oppenheimer (Eds), Volcanism and the Earth's Atmosphere. American Geophysical Union, Washington, DC, pp. 189–212.

Mavriplis, D.J., 1990. Adaptive mesh generation for viscous flows using Delaunay triangulation. J. Comput. Phys., 90: 271–291.

Mavriplis, D.J., 1995. Three-dimensional multigrid Reynolds-averaged Navier–Stokes solver for unstructured meshes. AIAA J., 33: 445–453.

Meneveau, C. and Katz, J., 2000. Scale-invariance and turbulence models for large-eddy simulation. Annu. Rev. Fluid Mech., 32: 1–32.

Meng, Z. and Seinfeld, J.H., 1996. Time scales to achieve atmospheric gas–aerosol equilibrium for volatile species. Atmos. Environ., 30: 2889–2900.

Morton, K.W., 1966. Numerical Solution of Convection–Diffusion Equations. Chapman & Hall, New York.

MPI-1, 1994. MPI Forum: A Message-Passing Interface Standard. Technical Report, University of Tennessee, Knoxville.

MPI-2, 1997. MPI-2 Forum: Extension to Message Passing Interface. Technical Report. University of Tennessee, Knoxville.

Murphy, D.M., 2005. Something in the air. Science, 307: 1888–1890.

NCAR, 2000. Fine-Scale Turbulence and Microphysics: Experiments and Measurements. In: R.A. Shaw (Ed.). Workshop on 'Fine Scale Turbulence and Cloud Microphysics'. NCAR, Boulder.

Neri, A., Esposti Ongaro, T., Macedonio, G. and Gidaspow, D., 2003. Multiparticles simulation of collapsing volcanic columns and pyroclastic flows. J. Geophys. Res., 108: B042202.

Neri, A. and Macedonio, G., 1996. Numerical simulation of collapsing volcanic columns with particles of two sizes. J. Geophys. Res., 101: 8153–8174.

Oberhuber, J.M., Herzog, M., Graf, H.F. and Schwanke, K., 1998. Volcanic plume simulation on large scales. J. Volcanol. Geotherm. Res., 87: 29–53.

Oberkampf, W.L. and Blottner, F.G., 1998. Issues in computational fluid dynamics code verification and validation. AIAA J., 36: 687–695.

Ollivier-Gooch, C. and Van Altena, M., 2002. A high-order-accurate unstructured mesh finite-volume scheme for the advection–diffusion equation. J. Comput. Phys., 181: 729–752.

Ongaro, T.E., Neri, A., Cavazzoni, C. and Erbacci, G., 2004. A parallel numerical code for the simulation of the transient, three-dimensional, multiphase flow dynamics of volcanic columns and pyroclastic flows. Proceedings of the CAPI 2004, 8 Workshop sul Calcolo ad Alte Prestazioni in Italia, November 24–25, Milano.

Ongaro, T.E., Neri, A., Todesco, M. and Macedonio, G., 2002. Pyroclastic flow hazard assessment at Vesuvius (Italy) by using numerical modelling. II. Analysis of flow variables. Bull. Volcanol., 64: 178–191.

OpenMP, 1997. OpenMP Forum: Fortran Language Specification, version 1.0, OpenMP Architecture Review Board. Lawrence Livermore National Laboratory, Livermore.

Ortigosa, E.M., Romero, L.F. and Ramos, J.I., 2001. Parallel simulation of spiral waves in reacting and diffusing media. Acta Cybernetica, 15: 173–184.

Ortigosa, E.M., Romero, L.F. and Ramos, J.I., 2003. Parallel scheduling of the PCG method for banded matrices arising from FDM/FEM. J. Parallel Distrib. Comput., 12: 1243–1256.

Papale, P. and Dobran, F., 1993. Modeling of the ascent of magma during the plinian eruption of Vesuvius in AD 79. J. Volcanol. Geotherm. Res., 58: 101–132.

Papale, P. and Dobran, F., 1994. Magma flow along the volcanic conduit during the plinian and pyroclastic flow phases of the May 18, 1980 Mount St. Helens eruption. J. Geophys. Res., 99: 4355–4373.

Passman, S.L., Nunziato, J.W. and Walsh, E.K., 1984. A theory of multiphase mixtures. In: C. Truesdell (Ed.), Rational Thermodynamics. Springer-Verlag (Springer), New York, pp. 286–325.

Peraire, J., Peiró, J. and Morgan, K., 1992. Adaptive remeshing for three-dimensional compressible flow computations. J. Comput. Phys., 103: 269–285.

Pilinis, C. and Seinfeld, J.H., 1988. Development and evaluation of an Eulerian photochemical gas–aerosol model. Atmos. Environ., 22: 1985–2001.

Pirzadeh, S., 1996. Three-dimensional unstructured viscous grids by the advancing-layers method. AIAA J., 34: 43–49.

Protezione Civile, 1995. Pianificazione Nazionale d'Emergenza dell'Area Vesuviana. Dipartimento della Protezione Civile, Roma.

Pruppacher, H.R. and Klett, J.D., 1997. Microphysics of Clouds and Precipitation. Kluwer, Dordrecht.

Pueschel, R.F. and Russell, P.B., 1994. Physical and optical properties of the Pinatubo volcanic aerosol: Aircraft observations with impactors and a sun-tracking photometer. J. Geophys. Res., 99: 12915–12922.

Ramanathan, V., Crutzen, P.J., Kiehl, J.T. and Rosenfeld, D., 2001. Aerosols, climate, and the hydrological cycle. Science, 294: 2119–2124.

Ramos, J.I., 1995. One-dimensional, time-dependent, homogeneous, two-phase flow in volcanic conduits. Int. J. Numer. Method. Fluid., 21: 253–278.

Ramos, J.I., 1999. Two-dimensional simulations of magma ascent in volcanic conduits. Int. J. Numer. Method. Fluid., 29: 765–789.

Ramos, J.I. and Soler, E., 2001. Domain-decomposition techniques for reaction–diffusion equations in two-dimensional regions with re-entrant corners. Appl. Math. Comput., 118: 189–221.

Reade, W.C. and Collins, L.R., 2000. Effect of preferential concentration of turbulent collision rates. Phys. Fluid., 12: 2530–2540.

Richardson, L.F., 1910. The approximate arithmetical solution by finite differences of physical problems involving differential equations, with an application to the stresses in a masonary dam. Trans. Roy. Soc. London, Series A, 210: 307–357.

Rizzi, A. and Vos, J., 1998. Towards establishing credibility in computational fluid dynamics simulations. AIAA J., 36: 668–675.

Roache, P.J., 1994. Perspective: A method for uniform reporting of grid refinement studies. J. Fluid. Eng., 116: 405–413.

Roache, P.J., 1998a. Verification and Validation in Computational Science and Engineering. Hermosa Publishers, Albuquerque.

Roache, P.J., 1998b. Verification of codes and calculations. AIAA J., 36: 696–702.

Robock, A., 2000. Volcanic eruptions and climate. Rev. Geophys., 38: 191–219.

Romero, L.F. and Zapata, E.L., 1995. Data distributions for sparse matrix vector multiplication. J. Parallel Comput., 21: 583–605.

Rosi, M., 1992. A model for the formation of vesiculated tuff by the coalescence of accretionary lapilli. Bull. Volcanol., 54: 429–434.

Rose, W., Delene, D., Schneider, D., Bluth, G., Krueger, A., Sprod, I., McKee, C., Davies, H. and Ernst, G., 1995. Ice in the 1994 Rabaul eruption cloud: Implications for volcano hazard and atmospheric effects. Nature, 375: 477–479.

Rose, W.I., Wunderman, R.L., Hoffman, M.F. and Gale, L., 1983. A volcanologist's review of atmospheric hazards of volcanic activity: Fuego and Mount St. Helens. J. Volcanol. Geotherm. Res., 17: 133–157.

Saad, Y., 1989. Krylov subspace methods on supercomputers. SIAM J. Sci. Stat. Comput., 10: 1200–1232.

Saad, Y., 2003. Iterative Solution Methods for Sparse Linear Systems. SIAM, Philadelphia.

Saad, Y. and Schultz, M.H., 1986. GMRES: A generalized minimal residual algorithm for solving nonsymmetric linear systems. SIAM J. Sci. Stat. Comput., 7: 856–869.

Scaillet, B., Luhr, J.F. and Carroll, M.R., 2003. Petrological and volcanological constraints on volcanic sulfur emissions to the atmosphere. In: A. Robock and C. Oppenheimer (Eds), Volcanism and the Earth's Atmosphere. American Geophysical Union, Washington, DC, pp. 11–40.

Schumacher, R. and Schmincke, H.U., 1995. Models for the origin of accretionary lapilli. Bull. Volcanol., 56: 626–639.

Seinfeld, J.H. and Pandis, S.N., 1998. Atmospheric Chemistry and Physics. Wiley, New York.

Shadid, J.N., 1999. A fully coupled Newton–Krylov solution method for parallel unstructured finite element fluid flow, heat and mass transfer simulations. Int. J. CFD, 12: 199–211.

Shadid, J.N., Tuminaro, R.S. and Walker, H.F., 1997. An inexact Newton method for fully coupled solution of the Navier–Stokes equations with heat and mass transport. J. Comput. Phys., 137: 155–185.

Shaw, R.A., 2003. Particle-turbulence interactions in atmospheric clouds. Annu. Rev. Fluid Mech., 35: 183–227.

SHMEM 1994. SHMEM User's Guide. SN-2516 version 1.1, Technical Report. Cray Research Inc., Seattle.

Shephard, M.S. and Georges, M.K., 1991. Automatic three-dimensional mesh generation by the finite Octree technique. Int. J. Numer. Method. Eng., 32: 709–747.

Sheridan, M.F. and Wohletz, K.H., 1983. Origin of accretionary lapilli from the Pompeii and Avellino deposits. In: R. Gooley (Ed.), Microbeam Analysis, San Francisco, pp. 35–38.

Shu, C.-W., 1996. Essentially non-oscillatory and weighted essentially non-oscillatory schemes for hyperbolic conservation laws. In: B. Cockburn, C. Johnson and C.-W. Tadmore (Eds), Advanced Numerical Approximations of Nonlinear Hyperbolic Equations. Lecture Notes in Mathematics, Springer-Verlag, New York, vol. 1697, pp. 325–432.

Smagorinsky, J., 1993. Some historical remarks of the use of nonlinear viscosities. In: B. Galperin and S.A. Orszag (Eds), Large Eddy Simulation of Complex Engineering and Geophysical Flows. Cambridge University Press, Cambridge, pp. 3–36.

Sreenivasan, K. and Antonia, R.A., 1997. The phenomenology of small-scale turbulence. Annu. Rev. Fluid Mech., 29: 435–472.

Sweby, P.K., 1984. High resolution schemes using flux-limiters for hyperbolic conservation laws. SIAM J. Numer. Anal., 21: 995–1011.

Syamlal, M., 1998. MFIX Documentation Numerical Technique. Department of Energy Report DE-AC21-95MC31346-01, Morgantown.

Symonds, R.B., Gerlach, T.M. and Reed, M.H., 2001. Magmatic gas scrubbing: Implications for volcano monitoring. J. Volcanol. Geotherm. Res., 108: 303–341.

Tabazadeh, A. and Turco, R.P., 1993. Stratospheric chlorine injection by volcanic eruptions: HCl scavenging and implications for ozone. Science, 260: 1082–1086.

Tai, C.H. and Zhao, Y., 2003. Parallel unsteady incompressible viscous flow computations using an unstructured multigrid method. J. Comput. Phys., 192: 277–311.

Textor, C. and Ernst, G.G.J., 2004. Comment on 'Particle aggregation in volcanic eruption columns' by G. Veitch and A.W. Woods. J. Geophys. Res., 109: B05202.

Textor, C., Sachs, P.M., Graf, H.F., and Hansteen, T.H., 2003. In: C. Oppenheimer, D.M. Pyle and J. Barclay (Eds), Volcanic Degassing. The Geological Society, London, pp. 307–328.

Thacker, W.C., 1980. A brief review of techniques for generating irregular computational grids. Int. J. Numer. Method. Eng., 15: 1335–1341.

Thompson, J.F., 1987. A composite grid generation code for general 3-D regions. AIAA paper 87-0275, AIAA 25th Aerospace Sciences Meeting, Reno.

Todesco, M., Neri, A., Ongaro, T.E., Papale, P., Macedonio, G., Santacroce, R. and Longo, A., 2002. Pyroclastic flow hazard assessment at Vesuvius (Italy) by using numerical modeling: I. Large-scale dynamics. Bull. Volcanol., 64: 155–177.

Valentine, G.A. and Wohletz, K.H., 1989. Numerical models of plinian eruption columns and pyroclastic flows. J. Geophys. Res., 94: 1867–1887.

Veitch, G. and Woods, A.W., 2001. Particle aggregation in volcanic eruption columns. J. Geophys. Res., 106: 26425–26441.

Wagner, G.J. and Liu, W.K., 2000. Turbulence simulation and multiple scale subgrid models. Comp. Mech., 25: 117–136.

Wagner, P.E., 2000. What do we know about phase transition processes relevant to atmospheric aerosols?. In: B.N. Hale and M. Kulmala (Eds), Nucleation and Atmospheric Aerosols 2000. American Institute of Physics, Melville, pp. 561–564.

Walker, G.P., 1981. Generation and dispersal of fine ash and dust by volcanic eruptions. J. Volcanol. Geotherm. Res., 11: 81–92.

Wang, L.-P., Wexler, A.S. and Zhou, Y., 2000. Statistical mechanical description and modeling of turbulent collision of inertial particles. J. Fluid Mech., 415: 117–153.

Warshaft, Z., 2000. Passive scalars in turbulent flows. Annu. Rev. Fluid Mech., 32: 203–240.

Zuccaro, G. and Ianniello, D., 2004. Interaction of pyroclastic flows with building structures in an urban settlement: A fluid-dynamic simulation impact model. J. Volcanol. Geotherm. Res., 133: 345–352.